

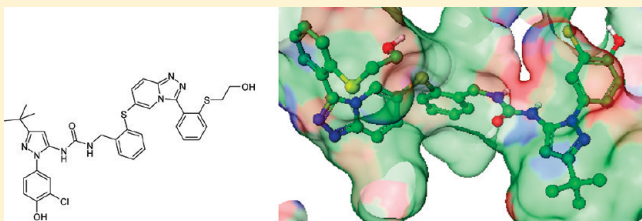
Design and Synthesis of Inhaled p38 Inhibitors for the Treatment of Chronic Obstructive Pulmonary Disease^{†,‡}

David S. Millan,^{*,§} Mark E. Bunnage,[§] Jane L. Burrows,[∞] Kenneth J. Butcher,[§] Peter G. Dodd,[§] Timothy J. Evans,[§] David A. Fairman,[⊥] Samantha J. Hughes,[§] Iain C. Kilty,^{||} Arnaud Lemaitre,[§] Russell A. Lewthwaite,[§] Axel Mahnke,[#] John P. Mathias,[§] James Philip,^{||} Robert T. Smith,[§] Mark H. Stefaniak,[§] Michael Yeadon,^{||} and Christopher Phillips[§]

[§]Worldwide Medicinal Chemistry, ^{||}Allergy and Respiratory Research Unit, [⊥]Department of Pharmacokinetics, Dynamics, and Metabolism, [#]Department of Drug Safety, and [∞]Department of Pharmaceutical Sciences, Pfizer Global Research and Development, Sandwich Laboratories, Ramsgate Road, Sandwich, Kent, CT13 9NJ, U.K.

Supporting Information

ABSTRACT: This paper describes the identification and optimization of a novel series of DFG-out binding p38 inhibitors as inhaled agents for the treatment of chronic obstructive pulmonary disease. Structure based drug design and “inhalation by design” principles have been applied to the optimization of the lead series exemplified by compound **1a**. Analogues have been designed to be potent and selective for p38, with an emphasis on slow enzyme dissociation kinetics to deliver prolonged lung p38 inhibition. Pharmacokinetic properties were tuned with high intrinsic clearance and low oral bioavailability in mind, to minimize systemic exposure and reduce systemically driven adverse events. High CYP mediated clearance and glucuronidation were targeted to achieve high intrinsic clearance coupled with multiple routes of clearance to minimize drug–drug interactions. Furthermore, pharmaceutical properties such as stability, crystallinity, and solubility were considered to ensure compatibility with a dry powder inhaler. **1ab** (PF-03715455) was subsequently identified as a clinical candidate from this series with efficacy and safety profiles confirming its potential as an inhaled agent for the treatment of COPD.

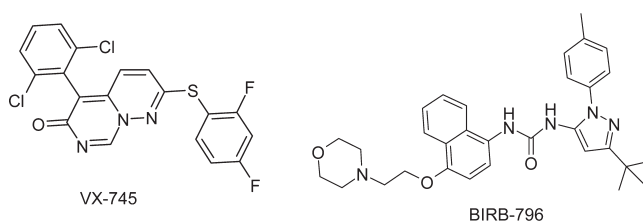


INTRODUCTION

p38 Mitogen activated kinase (MAP) is a ubiquitous target in the research based pharmaceutical industry. It plays a central role in the regulation of biosynthesis and actions of key proinflammatory mediators such as IL1- β and TNF- α . These cytokines, and others, are important regulators of the immune response to infection as well as cellular stress.¹ Indeed biologics that bind or remove TNF- α , such as etanercept, infliximab, and adalimumab, have shown good efficacy in the clinic.² Similarly, the IL-1 receptor antagonist anakinra has proved to be efficacious in rheumatoid arthritis (RA), suggesting that modulating the levels of these proinflammatory cytokines provides clinical benefit in inflammatory disorders.²

Small molecule inhibitors of p38, such as VX-745³ and BIRB-796⁴ (Chart 1), have advanced to clinical trials in inflammatory diseases, with VX-745 demonstrating significant clinical benefit in RA in a 12-week study. However, despite promising preclinical and clinical efficacy with several other oral p38 inhibitors, their progression to phase III studies and beyond has been hampered by adverse findings, such as skin disorders, infection, and a lack of sustained efficacy in diseases such as RA.⁵ The aforementioned inhibitor VX-745 was not progressed beyond the phase II RA trial because of CNS toxicity observed preclinically.⁶ Moreover, elevations in liver transaminases were observed, which declined

Chart 1



rapidly after cessation of dosing.³ Elevations of liver transaminases were also observed for BIRB-796 in a phase I 7-day multidose study.⁷ BIRB-796 progressed to a phase II study in Crohn's disease patients but failed to show clinical benefit.⁴ The compound is no longer listed on the companies' development pipeline, and it is assumed that it has been discontinued from further development.⁸

Perhaps more worrying is a common feature observed in many of the clinical trials run with several different p38 inhibitors, which could be linked to the disappointing efficacy observed.

Received: May 27, 2011

Published: September 05, 2011

In many of these studies a drop in C-reactive protein (CRP) levels (inflammatory biomarker) on drug treatment was observed, but this was not sustained after 2 weeks of dosing, suggesting possible redundancy in the p38 pathway.⁵ At this stage it is unclear whether this transient effect on serum biomarkers as well as the plateauing of clinical response is RA specific or not, and therefore, there has been significant effort in the pharmaceutical industry to investigate p38 inhibition in other inflammatory indications. Many respiratory diseases also show a significant inflammatory component, such as chronic obstructive pulmonary disease (COPD) and asthma. The global prevalence of COPD has reached epidemic proportions and is now one of the leading causes of death in the developed world.⁹ Existing treatments for COPD patients are dominated by long acting bronchodilators, with anti-inflammatory agents such as inhaled corticosteroids being largely ineffective in treating the inflammation or progression of the disease.¹⁰ There is therefore a huge unmet medical need with regard to effective anti-inflammatory agents to treat COPD patients.

Studies have demonstrated that p38 is activated in the alveolar macrophages of COPD patients, relative to control subjects, suggesting a link with the disease phenotype.¹¹ Small molecule inhibitors of p38 have also provided supporting evidence that modulating this pathway has the potential to show efficacy in respiratory diseases where inflammation is a key driver. Oral dosing of SB-239063 has been shown to reduce eosinophil infiltration following challenge with lipopolysaccharide (LPS) and also reduced the levels of IL-6 and MMP-9 in lavage fluid.¹² Another small molecule p38 inhibitor, SD-282, was efficacious in a mouse tobacco smoke model in which glucocorticoids were ineffective (Chart 2).¹³ Inhalation as a route of delivery has also been explored with a p38 α selective oligonucleotide which has shown efficacy when delivered to the lung in a model of asthma in the mouse.¹⁴ Similarly, when a small molecule inhibitor of p38 (ARRY-371797, structure not disclosed) was dosed directly to the lung, it was shown to significantly reduce levels of proinflammatory

cytokines, as well as neutrophil infiltration, in response to LPS challenge.¹⁵

Several oral p38 inhibitors have advanced to human clinical trials for COPD. PH-797804, losmapimod, and dilmapiomod (Chart 3) have all completed phase II trials for COPD.¹⁶ Results from the phase II trial of PH-797804 suggest real promise.¹⁷ In a 6-week study involving 230 patients, PH-797804 showed statistically significant improvements in FEV₁ (forced expiratory volume in 1 s) and clinically meaningful increases were observed on the transitional dyspnoea index. Interestingly, CRP levels remained low over the time course of the trial, and therefore, this result deviates from that seen in RA with other p38 inhibitors. However, it is reiterated that there is no credible reason why p38 pathway redundancy may not be observed in COPD, and therefore, it remains a significant risk. Longer clinical trials will help to answer this question. PH-797804 was also safe and well tolerated with p38 related adverse events such as skin rash observed in only approximately 7% of PH-797804 treated patients. To the best of our knowledge, data from other COPD studies, with other p38 inhibitors, have not been reported.

This promising result, as well as other preclinical studies discussed above, has prompted interest in the topical application of a p38 inhibitor directly to the lung of a COPD patient. Inhalation of a p38 inhibitor represents an intriguing opportunity to deliver powerful anti-inflammatory activity coupled with the potential to minimize systemically driven adverse events that may be p38 mechanism related.^{18,19} This paper will detail efforts to identify a potent, selective, and safe p38 inhibitor with pharmacokinetic and pharmaceutical properties suitable for lung delivery. The design principles adopted follow the “inhalation by design” philosophy outlined in a previous publication.²⁰

CHEMISTRY

The synthetic strategy for preparation of target compounds **1a–ac** in this paper is based on the same general disconnection for each analogue. This involves synthesis of the benzylamines **2a–h**, which is then coupled with either a commercially available or synthesized arylpyrazole **3a–k** through a urea forming step (Scheme 1).

The arylpyrazole portion of the target molecule was prepared by cyclocondensation of an arylhydrazine with a ketonitrile. The ketonitrile either was commercially available, as in 4,4-dimethyl-3-oxopentenenitrile, or was prepared from the corresponding commercially available precursors to afford **5a** and **5b** (Scheme 2). The ketonitrile **5a** was prepared from commercially available ethyl 2-methyl-2-(methylthio)propionate by reaction with the anion of acetonitrile. Similarly ketonitrile **5b** was prepared by

Chart 2

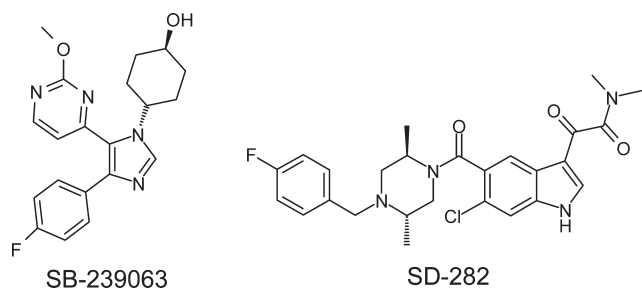
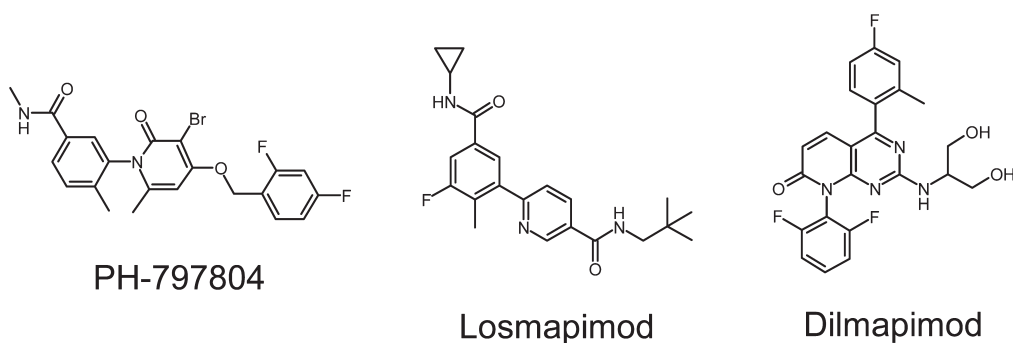
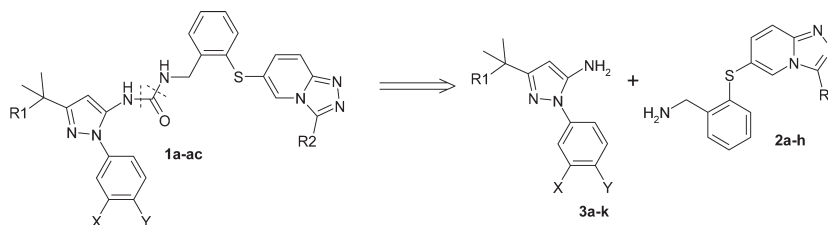
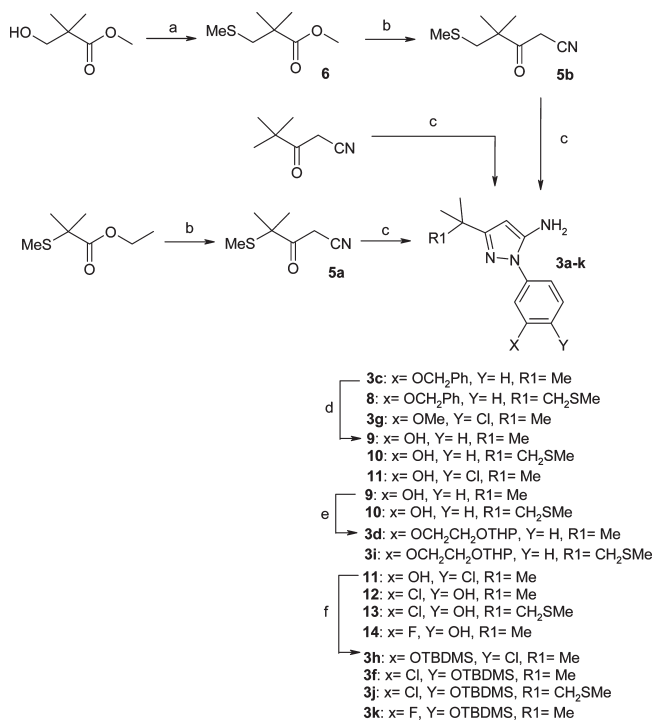


Chart 3



Scheme 1. General Retrosynthetic Strategy for Preparation of Target Compounds

Scheme 2^a

^a Reagents: (a) (i) ^tPrNEt₂, MeSO₂Cl, DCM, 0 °C, 2 h; (ii) MeSNa, MeOH, reflux, 17 h, 17%; (b) NaH, CH₃CN, THF, reflux, 5 h, 58–81%; (c) arylhydrazine, conc HCl, EtOH, reflux, 6 h, 23–95%; (d) BBr₃, DCM, 0 °C, 0.5 h, 18–89%; (e) THPOCH₂CH₂Br, K₂CO₃, DMF, 60 °C, 4 h, 71%; (f) TBDMSCl, imidazole, DMF, room temp, 16 h, 17–93%.

reaction of the commercially available methyl 2,2-dimethyl-3-hydroxypropionate with methanesulfonyl chloride followed by nucleophilic displacement with the sodium salt of methanethiol, affording **6**. This was followed by reaction with the anion of acetonitrile to afford the corresponding ketonitrile **5b**.

Arylhydrazines **4a** and **4b** were not commercially available and were therefore prepared from the corresponding commercially available aryl bromides (Scheme 3). First, 5-bromo-2-chloroanisole was metalated with *n*-butyllithium followed by reaction with di-*tert*-butyl diazodicarboxylate to afford the corresponding diazo compound, which was deprotected in situ with hydrochloric acid, affording the hydrazine hydrochloride salt **4a**. **14** was prepared by a similar procedure as above, but first isolating **7** followed by in situ deprotection with hydrochloric acid and reaction with commercially available 4,4-dimethyl-3-oxopentanenitrile. Alternatively, the arylhydrazine **4b** could be prepared from the commercially

available 4-amino-2-chlorophenol, by diazotization, followed by tin chloride mediated reduction of the diazo intermediate to furnish the desired hydrazine **4b** (Scheme 3). The arylpyrazoles **3a–k** were prepared by cyclocondensation of the ketonitrile with the appropriate arylhydrazine, followed by deprotection and alkylation, affording **3d** and **3i**, or protection as silyl ethers, affording **3f**, **3h**, **3j**, **3k** (Scheme 2).

The benzylamines **2a–h** were synthesized by reaction of commercially available 5-bromo-2-hydrazinylpyridine with various commercially available aliphatic and aromatic aldehydes to afford the corresponding hydrazones **15a–d** in good yields (Scheme 4). The hydrazone was then reacted with iodobenzene diacetate in a cyclo-oxidation reaction to afford the bromotriazolopyridines **16a–g**. Reaction with commercially available 2-mercaptobenzyl alcohol in a palladium catalyzed coupling afforded the benzyl alcohols **17a–g**. The alcohols **17a–g** were then converted to the benzylamines **2a–f** by reaction with methanesulfonic anhydride and displacement of the corresponding mesylate with ammonia in methanol. Finally, **2g** was prepared by debenzoylation of **2d** with boron tribromide.

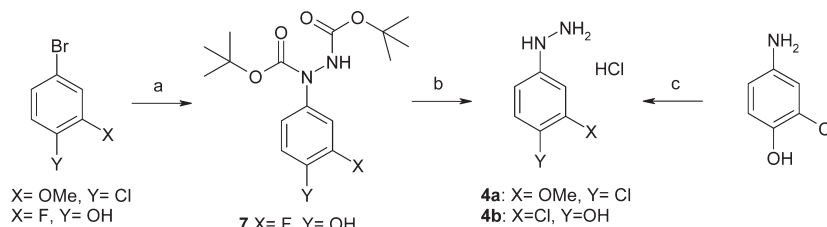
To install the hydroxyethylene group in **2h**, **2g** was reacted with di-*tert*-butyl dicarbonate to doubly protect the amine and phenol to afford **18**. A selective deprotection of the carbonate was achieved with sodium carbonate to afford **19**, followed by alkylation to give **20**. Deprotection of the primary amine and removal of the THP protecting group revealed the desired coupling partner **2h** (Scheme 5).

In several instances the aldehyde was not commercially available and was therefore synthesized. The aldehyde **21a** was prepared by benzyl protection of the commercially available 3-chlorosalicylaldehyde (Scheme 6).

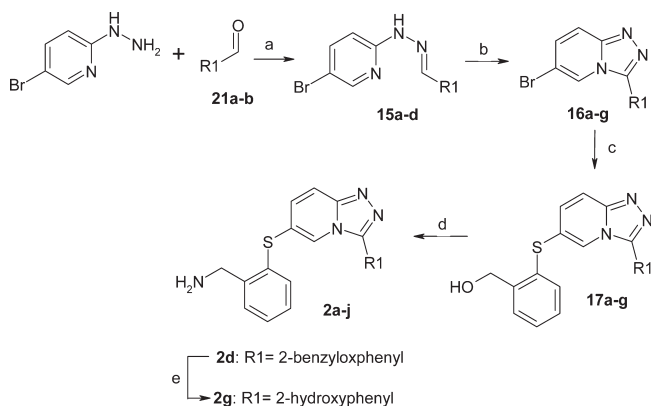
Aldehyde **21b** was prepared by taking commercially available methyl thiosalicylate and alkylating with (2-bromoethoxy)-*tert*-butyldimethylsilane to afford **22**. The ester was then reduced to afford the alcohol **23**, which was then oxidized to give the desired aldehyde **21b** (Scheme 7).

With benzylamines **2a–h** and the arylpyrazoles **3a–k** in hand we were able to conduct the urea forming reaction to synthesize target compounds **1a–ac**. This was achieved by one of two methods. We initially utilized carbonyldiimidazole as a carbonyl source to produce **1a–c**, **1j**, **1n–o**, **1y**, and **24–30**. **24–30** were then further manipulated to furnish target compounds **1e–f**, **1i**, **1k–1l**, **1p**, **1u** in good yield. (Scheme 8). Target compound **1y** did not require desilylation of the phenolic protecting group, as it was spontaneously removed during the urea forming step. The sulfoxides **1g**, **1m**, and **1q** were prepared by oxidation of **1f**, **1l**, and **1p**, respectively.

For the synthesis of advanced lead compounds such as **1d**, **1h**, **1r–t**, **1v–x**, **1z–ab** we first formed the phenyl carbamates **31a–e** of the arylpyrazoles **3c**, **3d**, **3f**, **3h**, **3j**, respectively, followed by

Scheme 3^a

^a Reagents: (a) *n*-BuLi, di-*tert*-butyl diazodicarboxylate, THF, $-78\text{ }^{\circ}\text{C}$, 2 h, 50%; (b) 4 M HCl, 1,4-dioxane, room temp, 16 h, 60%; (c) (i) conc HCl, NaNO_2 , H_2O , $-10\text{ }^{\circ}\text{C}$, 0.5 h, (ii) 6 N HCl, SnCl_2 , $-10\text{ }^{\circ}\text{C}$, 3.5 h.

Scheme 4^a

^a Reagents: (a) EtOH, reflux, 1 h, 86–99%; (b) $\text{PhI}(\text{OAc})_2$, DCM, EtOH, room temp, 18 h, 68–88%; (c) 2-mercaptobenzyl alcohol, $\text{Pd}(\text{dppf})_2\text{Cl}_2$, Cs_2CO_3 , DMF, $90\text{ }^{\circ}\text{C}$, 2 h, 17–77%; (d) (i) $(\text{Ms})_2\text{O}$, DCM, room temp, 2 h, (ii) 7 N NH_3/MeOH , room temp, 16 h, 38–98%; (e) BBr_3 , DCM, $0\text{ }^{\circ}\text{C}$, 0.5 h, 51%.

reaction of the carbamates with the benzylamines **2a–c** and **2g** to afford the desired target compounds in good yields (Scheme 9). Target compounds **1h**, **1v–x**, and **1aa–ab** did not require desilylation of the phenolic protecting group that was on **31c–e**, as it was spontaneously removed during the urea forming step.

RESULTS AND DISCUSSION

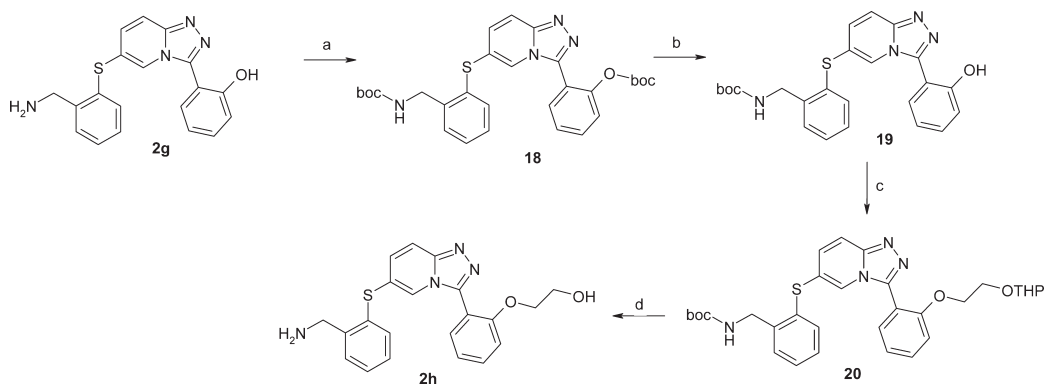
Alongside the essential characteristics of a successful drug, such as efficacy and safety, inhalation as a route of delivery requires a compound to have certain other attributes to increase the likelihood of success. These include (1) high potency to achieve a low inhaled dose (≤ 1 mg of drug product), (2) duration of action (DoA) for therapeutically relevant period, (3) high clearance and low oral absorption of any swallowed dose to minimize systemic exposure and therefore potential for adverse events, (4) multiple routes of clearance to minimize drug–drug interactions (DDIs), and (5) physical form characteristics suitable for a dry powder inhaler including high crystallinity and compatibility with lactose which is the commonly used excipient. These requirements suggest that designing compounds at the edge of or outside the “rule-of-five” (Ro5) would potentially increase the likelihood of achieving the pharmacokinetic profile mentioned above.²¹ Non-Ro5 physicochemical space could potentially deliver a compound with relatively higher clearance, through high lipophilicity, and a slower rate of absorption of drug from the lung to the systemic circulation through a reduction in

permeability and solubility. The latter concept could conceivably lead to increasing the duration of action (DoA) of the inhibitor at the site of action by retaining the compound in the lung.

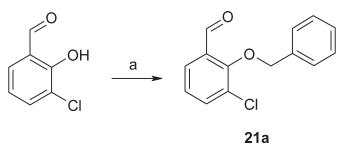
In addition to achieving a DoA by physical means, we hypothesized that a slow k_{off} from the enzyme itself could extend the DoA. The discovery of the oral p38 inhibitor BIRB-796 and its unique enzyme kinetics suggested that potent and selective p38 α inhibitors could be designed with the potential for a longer duration of action (DoA).^{22,23} The slow k_{on} and slow k_{off} rates observed with the inhibitor were rationalized on the basis of X-ray crystallographic observations. For BIRB-796 to bind to p38 α , it was reported that the activation loop (consisting of the conserved residues Asp168-Phe169-Gly170) must undergo a movement of about 10 Å, creating a lipophilic pocket that was then filled by the arylpyrazole moiety. High affinity binding to the so-called DFG-out conformation was reported to deliver the long k_{off} rates. For this reason we decided to target the DFG-out conformation.

At the time we were aware of a triazolopyridine series of DFG-in binding inhibitors of p38 that were highly selective because of a unique ability to act as a dihydrogen bond acceptor at the hinge region of the kinase due to an induced flip of Gly110.²⁴ A similar series containing a triazolopyridine, as exemplified by **41** (Chart 4), had also been published that contained a urea, similar to that in BIRB-796.²⁵ **41** has been cocrystallized in p38 α and was found to bind in the DFG-in conformation and as expected had relatively fast k_{on} and k_{off} rates, as determined by surface plasmon resonance (SPR) (Table 1). This prompted us to consider hybridizing **41** and BIRB-796 to see if a potent DFG-out binding compound could be achieved with enzyme kinetics similar to those of BIRB-796 (Figure 1). As can be seen from the overlay of **41** onto the cocrystal structure of BIRB-796 in p38 α , the N-3 of the triazolopyridine in **41** overlays well with the oxygen of the morpholino group in BIRB-796. These are the key hydrogen bond acceptors that make an interaction with Met109 at the hinge region of the kinase. The phenyl ring of **41** interacts with the gatekeeper residue (Thr106) and overlays well with the naphthalene ring system of BIRB-796, and finally the ureas of **41** and BIRB-796 are also suitably aligned. With these structural similarities in mind **1a** (Chart 4) was designed and synthesized and gratifyingly proved to be a potent p38 inhibitor with enzyme kinetics akin to those of BIRB-796 (Figure 2, Table 1).

The slow k_{on} and k_{off} rates presented a screening challenge at the outset of this program. We decided to use a cell based assay to routinely assess the potency of target compounds. Compounds were tested for their ability to inhibit TNF- α production from LPS stimulated human isolated peripheral blood mononuclear cells (PBMCs). First we needed to establish how long our whole

Scheme 5^a

^a Reagents: (a) (BOC)₂O, ^tPrNEt₃, DMF, room temp, 72 h, 100%; (b) Na₂CO₃, 1,4-dioxane, H₂O, 70 °C, 16 h, 87%; (c) THPOCH₂CH₂Br, NaH, *N*-methylpyrrolidinone, 55 °C, 16 h, 55%; (d) 4 M HCl, 1,4-dioxane, room temp, 2 h, 95%.

Scheme 6^a

^a Reagents: (a) benzyl bromide, K₂CO₃, THF, reflux, 30 h, 92%.

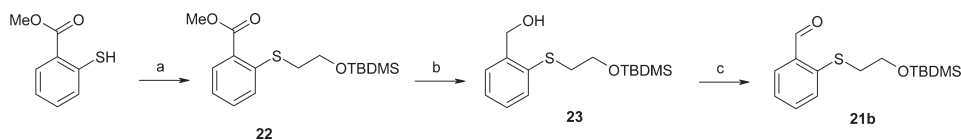
cell PBMC assay would need in terms of preincubation time to ensure that the experiment was at equilibrium. **1a**, for example, had an IC₅₀ in the whole cell assay of 5 nM after a 10 min preincubation time, whereas if the preincubation time was increased to 1 h, the IC₅₀ decreased to 0.3 nM. It did not decrease further with longer preincubation times. Therefore, a preincubation time of 1 h was used for future screening. This suggests that the slow *k*_{on} and *k*_{off} were clearly impacting the time to equilibrium in this experiment. With **1a** being potent in a cell based assay and having the desired enzyme kinetics, we were keen to investigate the selectivity profile against wider kinases. Through binding to the DFG-out region of the kinase it was hypothesized²⁶ that a good selectivity profile could be achieved, as many kinases in the kinase are potentially unable to adopt a DFG-out conformation. Interestingly, **41** being a DFG-in binding mode was more selective than the DFG-out binding mode observed with compound **1a**, which is contrary to the hypothesis above. It is possible that the kinases with significant inhibition at 10 μM (shown in red) are capable of binding in the DFG-out binding mode in a similar way to p38 (Figure 3).

With a promising lead in **1a** we sought to investigate and optimize the pharmacokinetic and pharmaceutical properties for inhalation while maintaining the high levels of potency and selectivity. As mentioned above, targeting high hepatic clearance was important for minimizing systemic exposure following absorption from the lung or absorption from the gut from any swallowed dose. In the targeting of liver metabolism, it was also key to ensure that the metabolites were inactive or had reduced activity and therefore could not contribute to any systemic p38 activity. With these considerations in mind we examined the cocrystal structure of **1a** in p38α which pointed to several opportunities to tune the pharmacokinetic properties of this series (Figure 4).

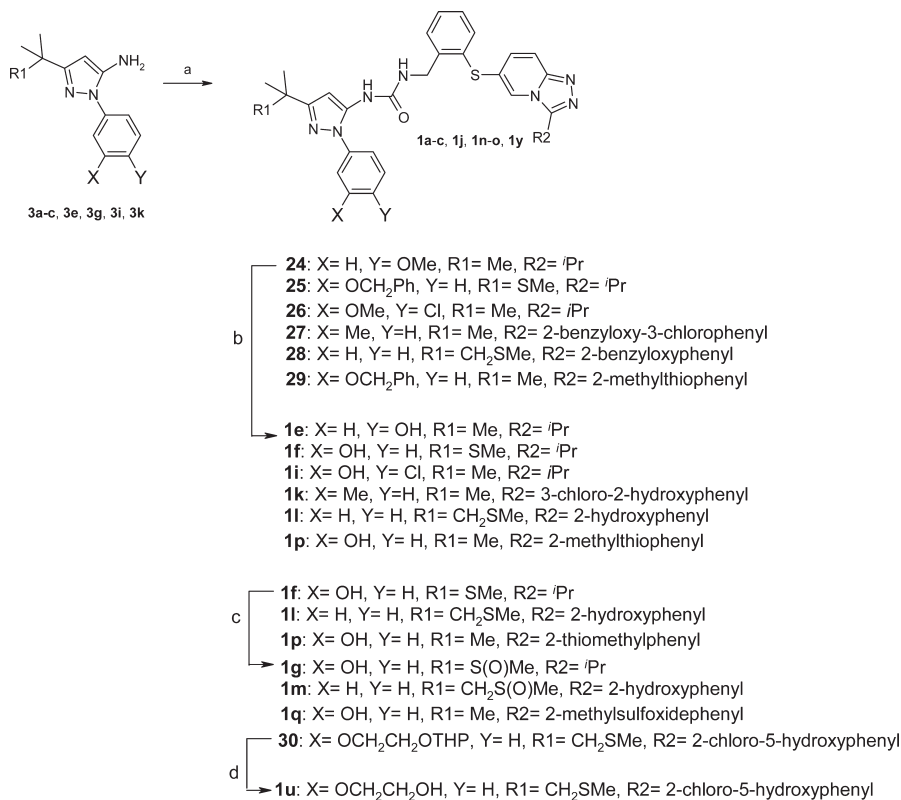
The *tert*-butyl group of **1a** resides in a lipophilic pocket created by activation loop movement. Introduction of a “soft” metabolic group within this pocket may render the molecule to site directed metabolism leading to a more polar metabolite having reduced binding affinity for p38. Alternatively the isopropyl group on the triazolopyridine of **1a** could be replaced with soft metabolic groups that may also lead to a less potent metabolite. These modifications would lead to phase I cytochrome P450 (CYP) mediated metabolism; therefore, to mitigate any CYP mediated DDI potential, we were interested in introducing the potential for phase II mediated metabolic pathways. Glucuronidation is a phase II metabolic pathway that has high capacity and is a major route of drug inactivation.²⁷ Phenol groups are well documented to undergo glucuronidation, and so we intended to explore the possibility of their introduction into synthetically accessible regions of the molecule that were also likely to be tolerated from a potency standpoint. The *N*-phenyl ring of the arylpyrazole moiety of **1a** was binding into a relatively hydrated pocket and therefore seemed a sensible site for the introduction of a phenolic group (Table 2).

As can be seen from compounds **1b–f,h,i**, generally good levels of potency could be achieved relative to the starting point **1a**. Introduction of a thiomethyl group at R², in **1b**, led to a slight drop-off in potency while a methylenethiomethyl, in **1c**, group led to a further drop-off in potency, suggesting that we were pushing the boundaries of the lipophilic pocket. It was gratifying to note that introduction of phenols in the meta and para positions of R¹ with **1d** and **1e**, respectively, did not lead to a significant drop-off in potency. Moreover, the combination of a thiomethyl group at R² with a *m*-phenol at R¹ retained good potency in **1f** alongside high intrinsic clearance. It was also pleasing to see some level of glucuronidation with this compound, although probably not enough to mitigate a CYP DDI. Interestingly, the corresponding proposed sulfoxide metabolite of this compound **1g** led to a significant drop-off in potency, thereby validating the hypothesis above. Introduction of a chlorine atom adjacent to the phenol in **1h** and **1i** resulted in potency akin to the starting point **1a** and displayed good levels of glucuronidation alongside high CYP mediated metabolism.

In parallel to the changes we were making on the arylpyrazole moiety we were interested in understanding if modifications of the isopropyl group on the triazolopyridine may also be useful.

Scheme 7^a

^a Reagents: (a) TBDMSOCH₂CH₂Br, NaH, DMF, room temp, 16 h, 81%; (b) (i) lithium aluminum hydride, THF, 0 °C → room temp, 16 h, 81%, (ii) Ba(MnO₄)₂, DCM, room temp, 24 h, (iii) MnO₂, DCM, reflux, 16 h, 62%.

Scheme 8^a

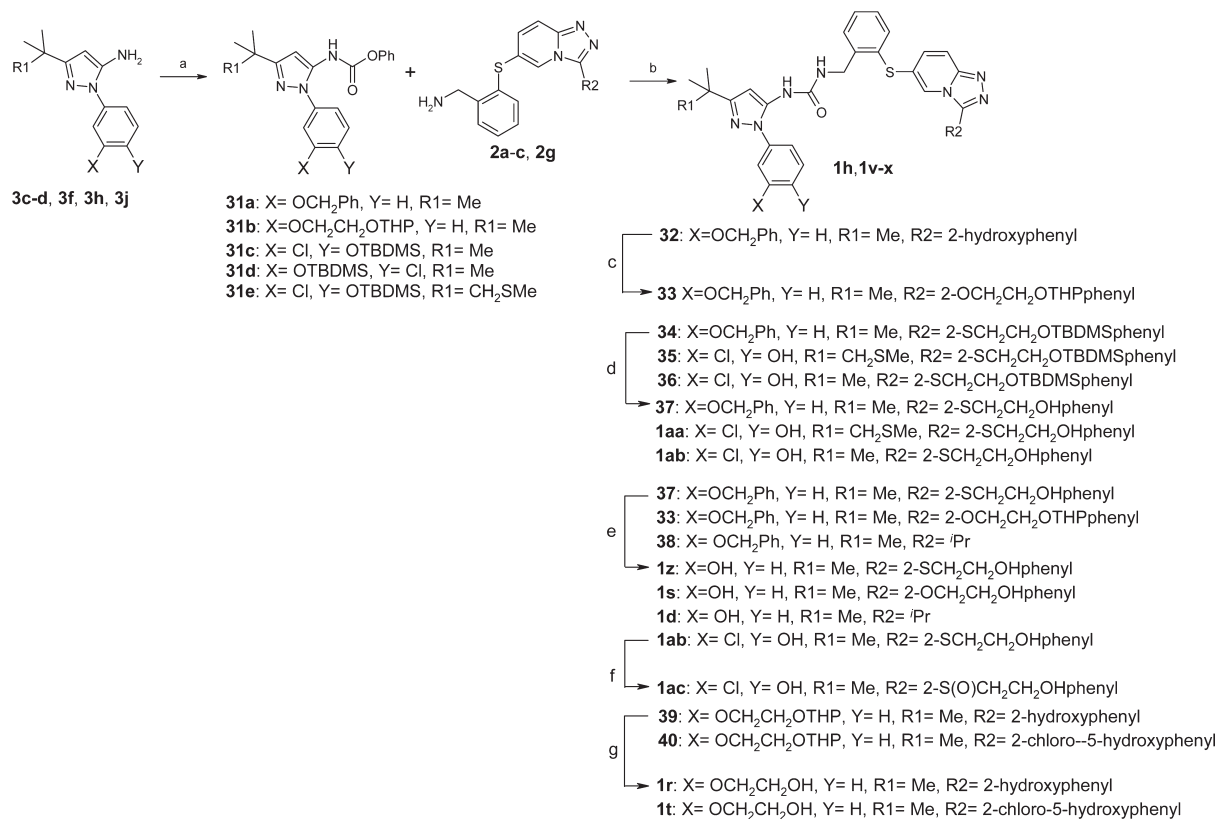
^a Reagents: (a) (i) CDI, DCM, room temp, 16 h, (ii) **2b–f**, **2h**, ⁱPrNEt₂, DCM, room temp, 1 h, 23–100%; (b) BBr₃, DCM, 0 °C, 0.5 h, 46–85%; (c) H₂O₂, 1,1,1,3,3,3-hexfluoropropan-2-ol, room temp, 0.5 h, 22–80%; (d) PTSA, MeOH, 60 °C, 3 h, 67%.

The cocrystal structure of **1a** suggested there was space to replace the isopropyl group with larger groups and in particular with a phenyl ring. To this end, we designed and synthesized **1j–s** (Table 3).

It was pleasing to note that **1j** retained good cellular potency after inclusion of a 2-hydroxyphenyl ring on the ATP binding portion of the molecule. **1k**, while also potent, demonstrated some level of glucuronidation, albeit low. Interestingly **1l** was more potent than **1c** seen previously, suggesting that on this scaffold the thiomethylmethylene group could be accommodated in the active site. Moreover, the sulfoxide metabolite **1m** of this compound led to a more than 100-fold drop-off in potency, which was encouraging from a metabolite activity perspective. The phenolic hydroxyl group could be moved around the phenyl ring in combination with a chloride substituent, in **1n** and **1o**, without loss of cellular potency. Alternatively the 2-hydroxyphenol could be replaced with a thiomethyl group in **1p**, again maintaining good cellular potency. The sulfoxide metabolite **1q**

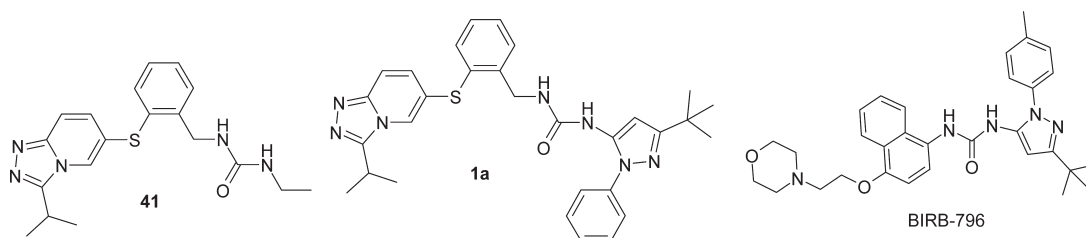
this time retained good potency with only a modest drop-off from its parent **1p**. **1p** and others above highlight that this region of the kinase binding site was very tolerant of functional groups of varying polarities and size and several different positions and hence represent a good opportunity to tune the physicochemical properties and in particular the properties required for inhalation. Finally introduction of a flexible hydroxyethylene group either on the phenyl ring at the DFG-out binding site, in **1r**, or at the ATP binding site, in **1s**, maintained good cellular potency despite being a relatively large group.

At this stage of the project we were interested to know whether the optimization of in vitro properties would translate into high clearance in vivo. To understand this, we investigated the intravenous and oral pharmacokinetic properties in rats (Table 4). The rat liver microsome (RLM) intrinsic clearance was high for **1f**, which translated into near liver blood flow clearance in the in vivo experiment and very high unbound clearance of >9600 (mL/min)/kg also. The high clearance and

Scheme 9^a

^a Reagents: (a) PhO(CO)Cl, pyridine, THF, 0 °C → room temp, 1 h, 86–100%; (b) ^tPrNEt₂, DMSO, room temp, 16 h, 23–96%; (c) THPOCH₂CH₂Br, K₂CO₃, DMF, 60 °C, 8 h, 75%; (d) triethylamine trihydrofluoride, MeOH, room temp, 16 h, 67–75%; (e) BBr₃, DCM, 0 °C, 0.5 h, 35–49%; (f) H₂O₂, 1,1,1,3,3,3-hexafluoropropan-2-ol, room temp, 0.5 h, 70%; (g) PTSA, MeOH, 60 °C, 3 h, 50–62%.

Chart 4



low volume of distribution of **1f** lead to a very short half-life in rat. The oral pharmacokinetics of **1f** suggests negligible oral bioavailability. This, of course, was exactly the pharmacokinetic profile we were targeting to minimize systemic exposure either through a lung absorbed fraction or an orally absorbed fraction following a swallowed dose.

Alongside favorable pharmacokinetic properties we were interested to know if the selectivity profile of **1f** was maintained from that of the original lead in **1a**. Indeed this was the case, with **1f** being only a potent inhibitor of isoforms of p38 (α , β , and γ) (Figure 5).

The favorable pharmacokinetic properties led us to evaluate some of the pharmaceutical properties of **1f** to see if the crystallinity, solid form properties, and solubility were commensurate with those required for inhalation. The powder X-ray diffraction

pattern of the crystalline **1f** suggested a good level of crystallinity, with a melting point of 220 °C, but the compound had no detectable solubility in water or in our simulated lung fluid (SLF) preparation. This was of great concern not only because dissolved material is required for a pharmacological response but also because this series of compounds appeared to have slow k_{on} and k_{off} rates, necessitating a relatively high local concentration to drive binding to the kinase. This prompted us to focus on looking for an inhibitor with an improved solubility profile. As a benchmark, we considered the marketed inhaled corticosteroid drug fluticasone as a good indicator of the required solubility we should be targeting in our SLF preparation (SLF \approx 0.5 μ g/mL).

In order to improve the solubility, we sought to disrupt the crystal packing of the molecule to a large enough extent such that the compound became more soluble but not so much that the

Table 1. p38 α Potency and Enzyme Kinetics

compd	k_{on} ($\text{M}^{-1} \text{s}^{-1}$)	k_{off} (s^{-1})	$t_{1/2}$ (h)	K_{D} (nM)	IC_{50} (nM) ^b
41 ^a	4.3×10^6	0.014	0.01	3.3	58
1a ^a	1×10^5	4×10^{-5}	4.81	0.4	0.3
BIRB-796 ^a	5×10^4	5×10^{-5}	3.85	1.0	15

^a Enzyme kinetics and K_{D} were determined by surface plasmon resonance using a Biacore instrument, on the inactive form of the kinase.

^b Compounds were routinely profiled by assessing their ability to inhibit TNF- α production from lipopolysaccharide (LPS) stimulated human isolated peripheral blood mononuclear cells (PBMCs), following a 1 h preincubation of PBMCs and test compound.

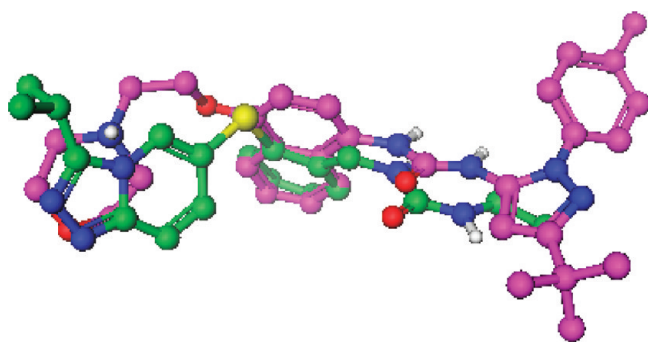


Figure 1. Overlay of 41 (carbon atoms colored green, derived from PDB entry 2yix) in the protein DFG-out cocrystal structure of BIRB-796 (carbon atoms colored purple) in p38 α (PDB entry 1kv2).

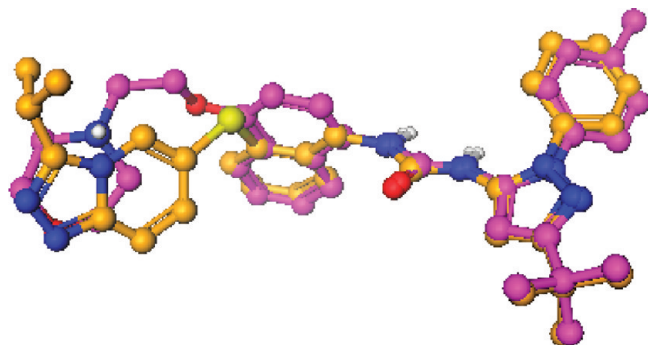


Figure 2. Overlay of 1a (carbon atoms colored orange, derived from PDB entry 2yix) in the protein DFG-out cocrystal structure of BIRB-796 (carbon atoms colored purple) in p38 α (PDB entry 1kv2).

compound became an amorphous solid. From our SAR studies we knew that the ATP binding site could tolerate groups such as hydroxyethylene in **1r** and **1s**, and we hypothesized that introduction of such flexible groups might disrupt the crystal packing enough to improve solubility to some extent. To this end, we crystallized compound **1r** and measured its SLF solubility, and we were pleased to see that we could now detect some dissolved material (SLF 1.0 $\mu\text{g}/\text{mL}$), which was above that of the benchmark fluticasone. As a result, **1r** became an attractive lead with good cellular potency, high intrinsic clearance, but unfortunately low levels of glucuronidation in the HLM UGT in vitro assay. In fact modeling of the DDI potential of **1r** did suggest that the lack of multiple routes of clearance for this compound could lead to it becoming a victim of a DDI. This led us to target higher rates of

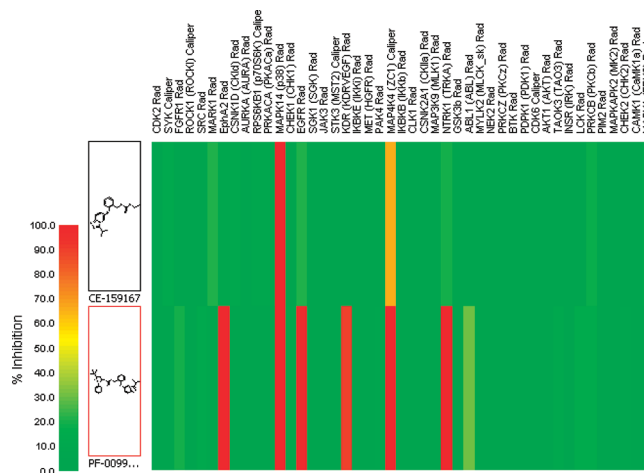


Figure 3. Selectivity profiles of 41 and 1a against a panel 45 kinases at 10 μM .

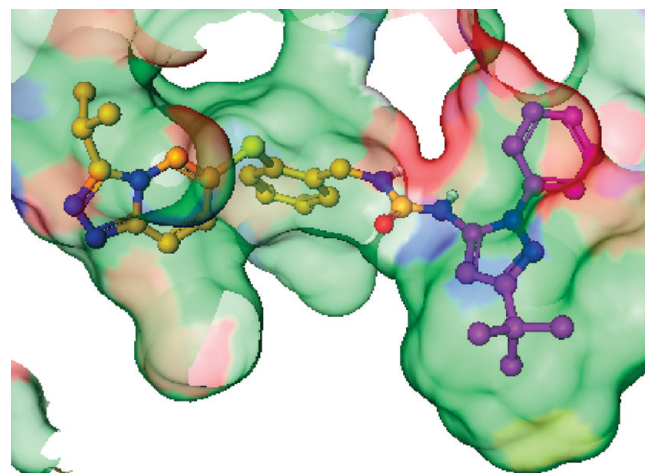
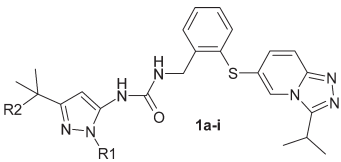


Figure 4. Binding site surface of 1a in p38 α cocrystal structure (PDB entry 2yix). The region of 1a highlighted in purple is binding into the pocket created by the DFG loop movement. Binding surface illustrates lipophilic surface (green/yellow), surface made up of hydrogen accepting oxygen atoms (red) and hydrogen donating atoms (blue).

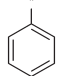
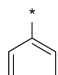
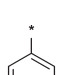
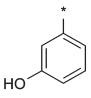
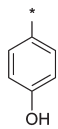
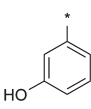
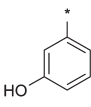
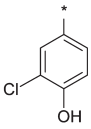
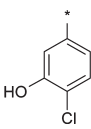
glucuronidation, alongside the other favorable characteristics observed in compound **1r**. **1t–ac** were designed and synthesized to address the above issues (Table 5).

1t and **1u** showed encouraging increases in glucuronidation rate relative to **1r**. However, significant improvement in glucuronidation rate came through the addition of 2-chlorophenol ring systems in **1v–x**. Interestingly **1v** and **1w** had differing rates of glucuronidation, suggesting that a *p*-phenol was preferred to maximize the rate of phase II metabolism. **1x** in particular was an interesting lead, as it had one of the highest rates of glucuronidation observed and also had very high cytochrome P450 driven metabolism, but unfortunately the addition of the methylenethiomethyl group at R^2 led to a significant drop-off in potency. Interestingly, the addition of a 2-fluorophenol in **1y** also led to a reduction in potency relative to the chloro analogue **1v**. It is interesting to note not only that the rates of glucuronidation appear dependent on the pK_{a} of phenol being glucuronidated but also that the compounds have SAR. This is probably not a surprise, as the

Table 2. p38 Potency, clogP, HLM, and HLM UGT Data for 1a–i



The chemical structure of 1a-i is shown above the table. It features a central benzimidazole ring system. One nitrogen is substituted with a tert-butyl group (R2) and the other with an R1 group. The benzimidazole ring is linked via a methylene group to a carbonyl group, which is further connected to a phenyl ring. This phenyl ring is substituted with a sulfur atom that is part of a thiazole ring system, which is also substituted with a tert-butyl group.

Compound	R1	R2	IC ₅₀ (nM) ^a	clogP	HLM ^b (μL/min/mg protein)	HLM UGT ^c (μL/min/mg protein)
1a		Me	0.8	6.9	>320	
1b		SMe	2.0	6.8	>320	1.7
1c		CH ₂ SMe	6.7	6.7		
1d		Me	1.1	6.3	385	
1e		Me	1.4	6.3	196	
1f		SMe	2.0	6.1	>440	2.0
1g		S(O)Me	74.0	3.6		
1h		Me	0.8	6.8	>287	155
1i		Me	0.8	6.8	303	66

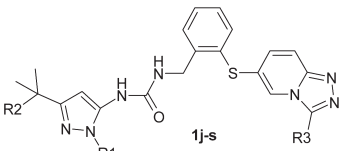
^a Compounds were routinely profiled by assessing their ability to inhibit TNF- α production from LPS stimulated human isolated PBMCs. ^b Compounds were routinely assessed for metabolic stability in human liver microsomes (HLM). ^c Compounds were assessed for phase II glucuronidation in HLM by including the cofactor uridine diphosphate glucuronic acid (UDPGA) and excluding the cytochrome P450 dependent cofactor NADPH.

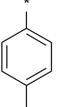
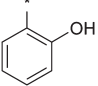
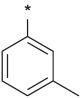
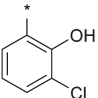
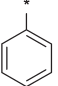
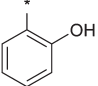
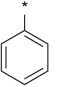
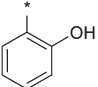
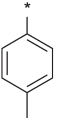
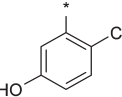
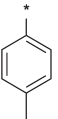
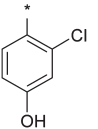
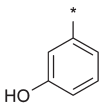
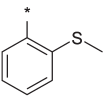
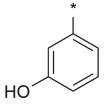
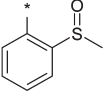
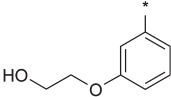
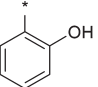
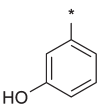
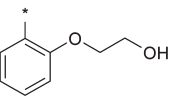
enzyme responsible for transferring the glucuronide to the xenobiotic compound will have a specific recognition element and therefore display SAR.

Several of the methylenethiomethyl analogues ($R^2 = \text{CH}_2\text{SMe}$), such as **1x**, were less potent than the *tert*-butyl analogue ($R^2 = \text{Me}$)

1v, and so we sought to incorporate a soft metabolic group in another part of the inhibitor to increase the chances of producing a significantly less active metabolite. **1p** had previously suggested that a thiomethyl group on the ATP binding side of the molecule was tolerated from a potency perspective but also

Table 3. p38 Potency, clogP, HLM, and HLM UGT Data for 1j–s



Compound	R1	R2	R3	IC ₅₀ (nM) ^a	clogP	HLM ^b (μL/min/mg protein)	HLM UGT ^c (μL/min/mg protein)
1j		Me		0.8	7.6	279	
1k		Me		2.7	8.1	126	41
1l		CH ₂ SMe		1.1	6.9	>440	27
1m		CH ₂ S(O)Me		155.0	4.7		
1n		Me		1.5	8.5	>440	43
1o		Me		1.7	8.5	132	
1p		Me		1.2	7.8	304	11
1q		Me		10.6	5.7		
1r		Me		0.8	6.8	>287	8
1s		Me		1.8	5.8	>320	

^a Compounds were routinely profiled by assessing their ability to inhibit TNF- α production from LPS stimulated human isolated PBMCs. ^b Compounds were routinely assessed for metabolic stability in HLM. ^c Compounds were assessed for phase II glucuronidation in HLM by including the cofactor UDPGA, excluding the cytochrome P450 dependent cofactor NADPH.

Table 4. In Vitro and in Vivo ADME Properties for **1f**

compd	iv clearance ^a ((mL/min)/kg)	V _{ss} (L/kg)	T _{1/2} (h)	oral bioavailability ^b (%)	PPB (%)	RLM ((μL/min)/mg protein)
1f	77	0.9	1	<5	>99	200

^aIntravenous (iv) pharmacokinetics were determined in rats from a 1 mg/kg dose. ^bOral pharmacokinetics were determined from a 3 mg/kg dose.

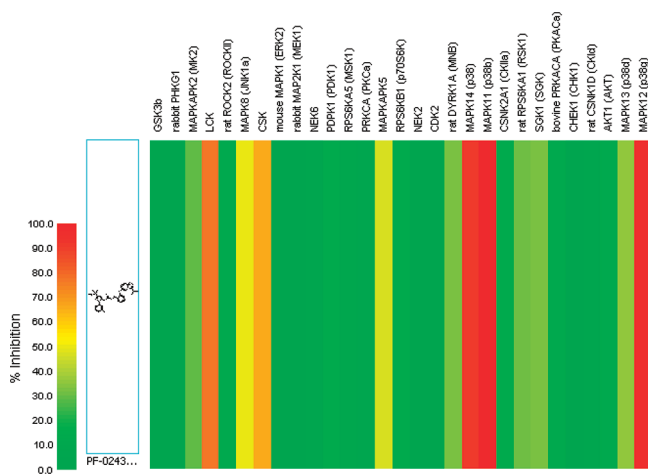


Figure 5. Selectivity profile of **1f** against a panel of 29 kinases, showing % inhibition at 10 μM.

that the metabolite **1q** only led to a modest drop-off in potency. This led us to design **1z** which incorporates both a soft metabolic handle and the flexible solubilizing hydroxyethyl chain. To improve on the glucuronidation rate of **1z**, we incorporated the more acidic phenol in **1aa** and **1ab** (PF-03715455), with **1ab** having the best balance of potency, HLM intrinsic clearance, and glucuronidation rate. The sulfoxide metabolite **1ac** also showed an approximate 25-fold drop-off in potency.

At this stage **1ab** was a very attractive lead, and so we set about characterizing it further. In the PBMC cell assay, with a preincubation time of 1 h the potency was determined to be 1.7 nM. Determining the potency of **1ab** against the human p38α enzyme proved to be complex as a result of the slow dissociation kinetics observed with this compound. The interaction of **1ab** with p38α was quantified by monitoring the IC₅₀ as a function of the preincubation time. In the presence of nonsaturating levels of ATP (10-fold below K_m, 5 μM ATP) a decrease in the IC₅₀ for **1ab** was observed from 9 nM (no preincubation) to 0.88 nM (40 min of preincubation).

The binding kinetics of **1ab** was determined for the inactive/nonphosphorylated form of human p38α using SPR. Fast k_{on} and slow k_{off} kinetics were observed with **1ab** for p38α, resulting in a half-life of approximately 80 h (Table 6). Clearly the enzyme kinetics for **1ab** is significantly different from that determined for **1a**, with a faster association rate and a slower dissociation rate, leading to a much greater affinity of **1ab** for the p38α enzyme, and a much slower half-life. The origin of this difference could not be rationalized easily from a structural perspective but could perhaps be due to the larger group at the 2-position of the triazolopyridine (2-hydroxyethylthiophenyl versus isopropyl) leading to improved affinity. The mismatch between K_D generated on **1ab** from binding kinetic constants and enzymatic IC₅₀ is attributed to the enzyme assay not being at equilibrium within a time frame suitable for enzymatic assays (maximum of 40 min). The relatively fast k_{on} of **1ab** coupled with the slow k_{off} rate

provides the optimal binding kinetics to overcome competition with high cellular levels of ATP. The potency and dissociation t_{1/2} of **1ab** for inhibiting rat p38α kinase were similar to the results observed for the human enzyme.

1a was shown to bind in the DFG-out binding mode which translated into slow dissociation kinetics, and so we were keen to confirm that the DFG-out binding mode was also apparent with **1ab**. Indeed, a protein cocrystal structure confirmed this to be the case (Figure 6).

The previous leads **1a** and **1f** displayed good selectivity profiles, and so we were keen to confirm that **1ab** was also selective over other kinases. **1ab** has an IC₅₀ at enzyme K_m for ATP of <1 μM for 15 enzymes of the 205 recombinant kinases screened. Scaling to the p38α IC₅₀ of 0.88 nM, five kinases have a selectivity ratio of ≤100×. Whole cell assays were established that demonstrated that recombinant enzyme activity does not translate to the whole cell for three of these kinases, leaving p38β (enzyme IC₅₀ = 23nM) and misshapen NIK related kinase 1 (MINK) (enzyme IC₅₀ 6nM) as potential cross over targets for **1ab**. Selectivity over p38β was not thought to represent a toxicity liability or be required for efficacy. The low systemic exposure expected for **1ab** coupled with the seemingly fast k_{on} and slow k_{off} kinetics for p38 suggested that inhibition of MINK is unlikely to represent a toxicity risk. Moreover, **1ab** did not inhibit LPS induced JNK phosphorylation (MINK signals through JNK) in the human monocytic cell line U937 at 1 μM, suggesting that **1ab** only inhibited p38 dependent end points.

In terms of physicochemical properties, **1ab** is a non-Ro5 compliant, high molecular weight (700 Da), highly lipophilic (clogP = 7.3, log D > 4.1), and weakly acidic molecule exhibiting an acidic pK_a of 7.45 (chlorinated phenol group). It therefore has low aqueous solubility (<0.1 mg/mL) but with measurable SLF solubility (3.0 μg/mL) when determined on a crystalline form. The pharmaceutical properties for **1ab** including crystallinity, stability on lactose, and solubility were considered suitable for dry powder inhalation.

The pharmacokinetics of **1ab** was then assessed in vitro and in vivo. **1ab** was rapidly metabolized in rat, dog, and human liver microsomes. The HLM glucuronidation experiment suggested that glucuronidation will significantly contribute to the human clearance of **1ab**. In fact the metabolite profile from human hepatocytes suggested that the glucuronide resulting from transfer to the chlorophenol is the major metabolite and presumably will be devoid or have greatly reduced p38 activity. In human hepatocytes, coadministration of 2 μM ketoconazole (CYP3A4 inhibitor) did not lead to any significant reduction in intrinsic clearance of **1ab** over the control incubations, suggesting that enzymes other than CYP3A4 contributed to the hepatocyte clearance of **1ab** with glucuronidation being a likely alternative pathway. These data suggest that **1ab** should not be a victim of a DDI. **1ab** is a moderate inhibitor of CYP1A2, CYP2C19, and CYP2D6 and a potent inhibitor of CYP's 2C9 and CYP3A4. However, on the basis of the very low projected unbound plasma C_{max} of **1ab**, the potential for the compound acting as a perpetrator of a DDI is low.

Table 5. p38 Potency, clogP, HLM, and HLM UGT Data for 1t–ac

1t-1ac

Compound	R1	R2	R3	IC ₅₀ (nM) ^a	clogP	HLM ^b (μL/min/mg protein)	HLM UGT ^c (μL/min/mg protein)
1t		Me		1.9	7.1	>285	53
1u		CH ₂ SMe		2.5	6.9	>216	47
1v		Me		3.5	6.3	202	130
1w		Me		1.9	6.3	232	70
1x		CH ₂ SMe		10.6	6.1	>440	310
1y		Me		22.0	5.9	>440	
1z		Me		1.5	6.8	>440	4
1aa		CH ₂ SMe		5.7	7.0		264
1ab		Me		1.7	7.3	>347	205
1ac		Me		40	5.8		

^a Compounds were routinely profiled by assessing their ability to inhibit TNF- α production from LPS stimulated human isolated PBMCs. ^b Compounds were routinely assess for metabolic stability in HLM. ^c Compounds were assessed for phase II glucuronidation in HLM by including the cofactor UDPGA, excluding the cytochrome P450 dependent cofactor NADPH.

Demonstrating intrinsic cell permeability was difficult to achieve with **1ab** because of its low solubility. However, as we were observing good levels of potency (<10nM) in our whole cell PBMC experiments, it is assumed that **1ab** has some level of intrinsic cellular permeability, although it is suggested to be low based on its physicochemistry. **1ab** is a high affinity substrate for P-glycoprotein (P-gp) ($K_m = 0.12 \mu\text{M}$). This, coupled with low solubility, and presumed low intrinsic permeability translated into negligible oral absorption in the rat (Table 7). Moderate total clearance was observed in rat and dog with **1ab**, but when corrected for high protein binding, this translates into extremely high unbound clearance values of 33 000 and 15 000 (mL/min)/kg, respectively. Human clearance predictions from preclinical data suggest low oral bioavailability and high clearance, resulting in a short half-life. Therefore, any drug reaching the systemic circulation, through absorption from either the gut or the lung, will be rapidly metabolized to relatively inactive metabolites.

With suitable pharmacokinetic properties demonstrated with **1ab**, we were then keen to assess if the overall properties of the molecule would translate into a desirable in vivo efficacy profile. LPS challenge to the lungs of rats results in lung neutrophilia, a characteristic of COPD, in addition to induction of both exhaled

nitric oxide and inflammatory mediator expression. When **1ab** was dosed as a micelle solution intratracheally (IT) 2 h prior to stimulus, it dose-dependently inhibited LPS induced lung neutrophilia with an efficacious dose (ED_{50}) of 30 μg . The maximum inhibition was similar to that of a solution dosed corticosteroid (fluticasone, dose 100 μg , 64% inhibition) of approximately 50–70%. To investigate the in vivo DoA of **1ab**, the compound was predosed for increasing times prior to LPS challenge. **1ab** showed significant inhibition of neutrophilia on 4 h of predosing but did not significantly inhibit lung neutrophilia on 24 h of predosing. To confirm that the apparent DoA of **1ab** was not due to systemic exposure, systemic anti-inflammatory activity was assessed in an ex vivo whole blood LPS induced TNF α assay. While a significant inhibition of ex vivo LPS induced TNF α production was observed 1 h after IT solution dosing, there was no significant inhibition in blood collected 4 h after dosing. These data suggest that the DoA observed in the LPS neutrophilia model was driven by sustained p38 α inhibition in the lung and was not due to systemic exposure (Figure 7). It is possible that this observed DoA is made possible by a combination of physical retention of the compound in the lung, as well as the slow dissociation kinetics from the p38 α enzyme.

1ab was subjected to wide ligand profiling (CEREP) at 10 μM which revealed <50% inhibition against 66 of the 68 targets assayed. IC_{50} values were therefore obtained for **1ab** at the N-type calcium channel (12 μM) and the human VEGFR1-tyrosine kinase (0.89 μM , consistent with findings in the kinase selectivity section). These affinities were all >1000 \times the primary pharmacology of **1ab** and therefore not considered a significant risk. Furthermore, **1ab** demonstrated little effect on the hERG current amplitude in the patch-clamp assay ($46 \pm 8.8\%$ inhibition at 10 μM ($n = 6$)) and no in vitro genetic toxicity was observed. Intravenous and oral in vivo toleration studies in the rat with **1ab** for 4 days did not induce any relevant clinical signs, clinical pathology, or histopathological evidence of toxicity at doses up to 2 and 2.8 (mg/kg)/day, respectively. Overall **1ab** had a preclinical safety profile suggesting it would be tolerated in humans at clinically relevant inhaled doses.

CONCLUSION

We have described our approaches toward the identification of a novel DFG-out binding lead series, beginning with **1a**, followed by subsequent optimization of various properties to ultimately identify **1ab**. Much of the design philosophy is similar to that described as “inhalation by design”, which was outlined in a previous publication.²⁰ **1ab** is a very potent and selective inhibitor for the p38 α enzyme, which translates into potent inhibition of proinflammatory cytokine release in whole cells that are relevant to COPD. Moreover, the enzyme kinetics of the inactivated form of the p38 α enzyme suggest fast association and slow dissociation, which should provide optimal binding kinetics to overcome competition with high cellular levels of ATP. In vivo experiments

Table 6. p38 α Affinity and Enzyme Kinetics of **1ab**

compd	k_{on} ($\text{M}^{-1} \text{s}^{-1}$)	k_{off} (s^{-1})	$t_{1/2}$ (h)	K_D (nM)
1ab ^a	3.1×10^6	2.4×10^{-6}	80	0.001

^a Enzyme kinetics were determined by surface plasmon resonance on the inactive form of the kinase using a Biacore instrument.

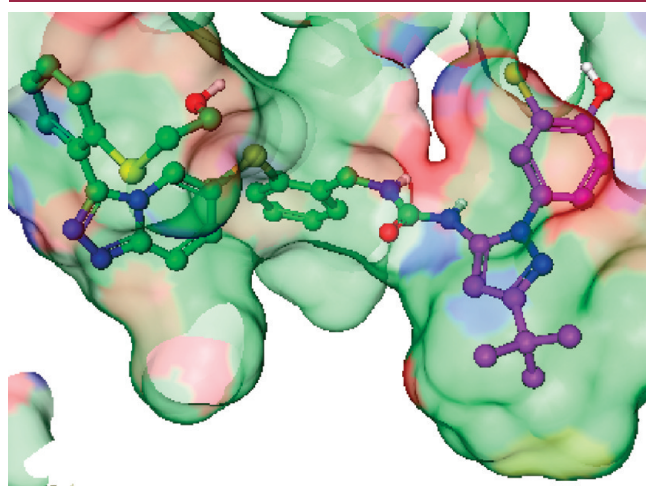


Figure 6. Binding site surface of **1ab** in p38 α cocystal structure (PDB entry 2yis). The region of **1ab** highlighted in purple is binding into the pocket created by the DFG loop movement. Binding surface illustrates lipophilic surface (green/yellow), surface made up of hydrogen acceptor atoms (red) and hydrogen donating atoms (blue).

Table 7. Intravenous (iv) and Oral Rat and Dog Blood Pharmacokinetics of **1ab**

species	dose (mg/kg)	iv clearance ((mL/min)/kg)	V_{ss} (L/kg)	$T_{1/2}$ (h)	oral absorption (%)	PPB (%)
rat iv ^a	1	33.8	0.19	1.0		99.8
rat po ^b	0.5				<5	99.8
dog iv ^c	0.48	13.1	0.06	0.5		99.9

^a Intravenous pharmacokinetics were determined in rats from a 1 mg/kg dose. ^b Oral pharmacokinetics were determined from a 0.5 mg/kg dose.

^c Intravenous pharmacokinetics were determined in dogs from a 0.5 mg/kg dose.

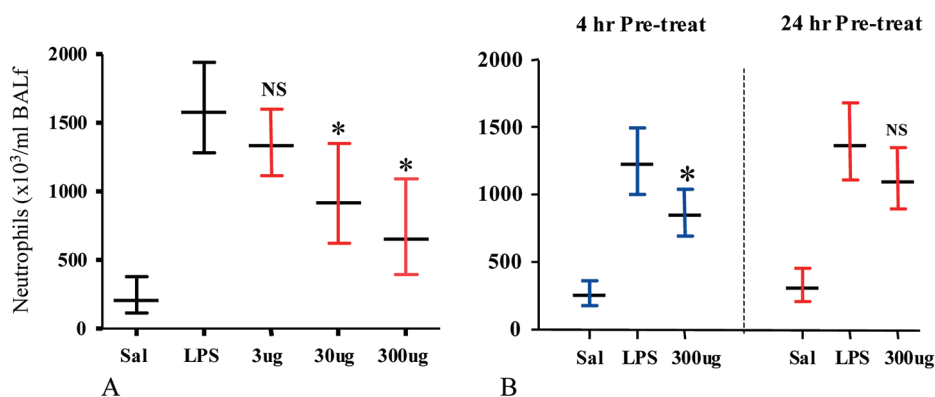


Figure 7. (A) Dose dependent inhibition of LPS induced neutrophilia at 2 h predosing with **1ab** and (B) demonstration of in vivo duration of action of greater than 4 h based on predosing studies: *, $p < 0.05$; NS, not statistically significant.

in rat suggest that **1ab** has a DoA greater than 4 h, which could be explained by slow dissociation kinetics in combination with physical retention of compound in the lung. The in vitro and in vivo pharmacokinetic profile suggests that the compound will display low oral bioavailability in humans following any swallowed dose, coupled with very high intrinsic clearance such that any lung absorbed drug will be rapidly metabolized to relatively inactive metabolites. Data suggest that **1ab** is metabolized by both phase I and phase II pathways and therefore should not be a victim or a perpetrator of any DDIs. The pharmaceutical properties of **1ab** are suitable for combination with lactose in a dry powder inhaler, with good stability, crystallinity, and solubility being key features. Finally the compound has demonstrated a good preclinical safety profile and may offer an improved safety profile relative to oral p38 inhibitors. This promising overall profile has led to the nomination of compound **1ab** as a development candidate for the treatment of COPD. Further information relating to the research and development of compound **1ab** will be reported in due course.

EXPERIMENTAL SECTION

Biology. In Vitro Pharmacological Activity. IC₅₀ Determination of Inhibition of TNF- α Release from Isolated Human Peripheral Blood Mononuclear Cells (PBMCs) after LPS Stimulation. Peripheral venous blood from healthy, nonmedicated donors was collected using ethylenediaminetetraacetic acid (EDTA) as the anticoagulant. For PBMC preparation, samples of blood were diluted 1:1 with sterile phosphate buffered saline and then separated using ACCUSPIN System-Histopaque-1077 tubes (Sigma-Aldrich, St. Louis, MO), centrifuged at 400g for 35 min. Buffy coat cells were removed into PBS, centrifuged at 200g for 10 min, and resuspended in PBMC assay buffer (Hanks balanced salt solution, 0.28% [w/v] 4-[2-hydroxyethyl]-1-piperazineethanesulfonic acid [HEPES], 0.01% [w/v] low-endotoxin bovine serum albumin [BSA]). A differential white cell count was performed, and PBMCs were diluted to 1×10^6 lymphocytes per mL in PBMC assay buffer. Test compounds were dissolved in DMSO and diluted in PBMC assay buffer (final DMSO concentration 1%) to cover an appropriate concentration range, e.g., 0.001–10000 nM. Samples of test compound solution or vehicle (20 μ L) were added into 96-well tissue culture treated plates (Corning), and PBMC (160 μ L) added to each well. The assay mixtures were incubated at 37 °C for 1 h in a humidified incubator containing an atmosphere of air supplemented with 5% CO₂ before adding LPS (20 μ L of 100 ng/mL). Plates were returned to the incubator for a further 18 h and then centrifuged

before recovery of samples of supernatant. TNF- α in the samples was determined using an enzyme-linked immunosorbent assay (ELISA) (Invitrogen kit no. CHC-1754; Invitrogen Carlsbad, CA) and following the manufacturer's instructions. Dose response curves were constructed from which IC₅₀ values were calculated. At least $n = 2$ determinations were made from a single donor of PBMCs. For compounds such as **1ab**, $n = 6$ determinations were conducted from six different donors, with IC₅₀ values ranging from 1.39 to 2.02 nM.

In Vivo Pharmacological Activity. ED₅₀ Determination of Inhibition of LPS-Induced Lung Neutrophilia in Rats. The primary objective of this procedure was to determine the anti-inflammatory activity of the compounds of formula 1, when administered directly into the lungs via the trachea, and also to determine the duration of effect. Test compounds were dissolved, or prepared as fine suspensions, in phosphate buffered saline containing 0.5% (w/v) Tween-80 to provide a range of dose levels. Male CD Sprague–Dawley rats (300–450 g) were randomized to study groups of $n = 6$ and then briefly anesthetized in an anesthetic chamber with 5% isoflurane in 3 L/min O₂. One of the test compound formulations or dose vehicle (100 μ L) was injected directly into the trachea of each anesthetized rat using a Hamilton syringe. The animals were then allowed to recover from the anesthetic. Dependent on the study design, animals were predosed 2, 4, or 24 h prior to inflammatory challenge. The rats were placed into a chamber (300 mm \times 300 mm \times 450 mm), connected to an ultrasonic nebulizer and a small animal rodent ventilator set to the maximum tidal volume and rate (5 mL, 160 strokes/min). An amount of 10 mL of 1 mg/mL LPS (Sigma-Aldrich, L2630) dissolved in saline, prewarmed to 37 °C, was nebulized into the chamber. After 15 min the ventilator and nebulizer were turned off, and the animals remained in the chamber to breathe the mist for a further 15 min before being returned to the home cage. Four hours after the end of the LPS treatment the animals were terminally anesthetised with 1 mL/kg Pentobarbital ip. The trachea was cannulated. The lungs were lavaged with 4×2.5 mL of PBS containing 2.6 mM EDTA, and the lavage fluid was collected. An amount of 1 mL of bronchioalveolar lavage (BAL) was added to 125 μ L of 40% bovine serum albumin (BSA) and the cellular count determined using an Advia 120 hematology system (Siemens). Also, a terminal blood sample was collected from each rat, and IC₅₀ was determined for inhibition of LPS induced TNF α release from whole blood. Dose response curves were constructed for inhibition of LPS-induced lung neutrophils, and half-maximal effect doses (ED₅₀) were estimated from the fitted curves.

p38 α Enzyme Kinetics (k_{on} and k_{off}) for PF-03715444 (1ab**), As Determined by Surface Plasmon Resonance Using a Biacore Instrument, on the Inactive (Nonphosphorylated) Form of the Kinase.** Biacore uses a technique based upon surface plasmon resonance to follow the real-time binding of compounds in a

liquid milieu to immobilized proteins on a carboxymethyl dextran surface. The compounds flow across the protein surface, and as they bind, there is an increase in signal (RU). Then, as the compounds dissociate from the surface, the signal decreases and returns to baseline. These binding studies were performed at 25 °C using a running buffer of 10 mM HEPES, 150 mM NaCl, 0.005% P20 with a flow rate of 20 μ L/min. For immobilization, a CMS chip (Biacore, Piscataway, NJ) was preconditioned and then streptavidin immobilized (13000–14000 RU) using amine coupling with *N*-hydroxysuccinimide and *N*-ethyl-*N'*-(3-dimethylaminopropyl)carbodiimide according to Biacore methods. Nonphosphorylated BirA-MK2 (control flow cell) or BirA-p38 α were then captured to a level of 10000–11000 RU. These particular binding experiments were done slightly differently from typical Biacore studies. To the immobilized, nonphosphorylated, and biotinylated p38 α was added SC-71830 (200 nM) which was first allowed to bind (three times) to achieve a maximal control response. SC-71830 is a proprietary ATP competitive p38 α inhibitor that displays fast on and fast off p38 α enzyme kinetics. In theory any fast on and fast off inhibitor that is ATP competitive could be used. Following dissociation of the final pass of SC-71830, **1ab** (1000 nM) was injected for 5 min. At various times after the injection of **1ab**, SC-71830 (200 nM) was injected and the binding response measured. As **1ab** dissociated from the immobilized p38 α , the binding of SC-71830 increased. The increase in binding response of SC-71830 over time was used to measure the dissociation of **1ab**, and these data were used to calculate the k_{on} and k_{off} for **1ab**.

Chemistry. Unless otherwise indicated, all reactions were carried out under a nitrogen atmosphere, using commercially available anhydrous solvents. “Ammonia” refers to commercially available aqueous ammonia solution of 0.880 specific gravity. Thin-layer chromatography was performed on glass-backed precoated Merck silica gel (60 F254) plates, and compounds were visualized using UV light, 5% aqueous potassium permanganate, or chloroplatinic acid/potassium iodide solution. Silica gel column chromatography was carried out using 40–63 μ m silica gel (Merck silica gel 60). Proton NMR spectra were measured on a Varian Inova 400 or Varian Mercury 400 spectrometer in the solvents specified. In these NMR spectra, exchangeable protons that appeared distinct from solvent peaks are also reported. Low resolution mass spectra were recorded on either a Fisons Trio 1000, using thermospray positive ionization, or a Finnigan Navigator, using electrospray positive or negative ionization. High resolution mass spectra were recorded on a Bruker Apex II FT-MS using electrospray positive ionization. Test compound purity of $\geq 95\%$ was determined using combustion analysis conducted by Exeter Analytical U.K. Ltd., Uxbridge, Middlesex, U.K. In the absence of test compound purity data determined by combustion analysis, all target compounds were purified until at least $\geq 95\%$ purity as judged by HPLC utilizing an ELSD detection system.

Methyl 2-[(2-[(*tert*-Butyl(dimethyl)silyl]oxy)ethyl]thio]benzoate (22**).** Sodium hydride (60% in oil, 1.70 g, 29.9 mmol) was washed with heptane and subsequently suspended in *N,N*-dimethylformamide (25 mL). To this was added methyl thiosalicylate (5.0 g, 29.9 mmol), and the mixture was allowed to stir for 1 h. A solution of (2-bromoethoxy)-*tert*-butyldimethylsilane (7.16 g, 29.9 mmol) in *N,N*-dimethylformamide (5 mL) was added dropwise, and the mixture was allowed to stir overnight at room temperature. The mixture was diluted with ethyl acetate (100 mL), and the organics were washed with brine (100 mL) and dried (MgSO₄). Concentration in vacuo gave a colorless oil (7.90 g, 81%). ¹H NMR (400 MHz, CDCl₃) δ 7.85 (dd, 1H), 7.32–7.39 (m, 2H), 7.97 (dt, 1H), 3.85 (s, 3H), 3.78 (t, 2H), 3.03 (t, 2H), 0.83 (s, 9H), 0.00 (s, 6H) ppm. LRMS: m/z 327 [M + H]⁺.

2-[(2-[(*tert*-Butyl(dimethyl)silyl]oxy)ethyl]thio]phenyl]methanol (23**).** To a solution of **22** (7.90 g, 24.37 mmol) in tetrahydrofuran (50 mL) at 0 °C was added lithium aluminum hydride (1 M in tetrahydrofuran, 24.37 mL, 24.37 mmol), and the mixture was allowed to warm to room temperature with stirring overnight. Water (1 mL) was added

dropwise to the mixture, followed by sodium hydroxide (1M, 3 mL). The mixture was then stirred for 30 min at room temperature. The mixture was filtered through Celite, and the Celite was then washed with ethyl acetate. The organics were then concentrated in vacuo to give a clear oil (5.90 g, 81%). ¹H NMR (400 MHz, CDCl₃) δ 7.39–7.45 (m, 1H), 7.32–7.35 (m, 1H), 7.16–1.26 (m, 2H), 4.74 (s, 2H), 3.71 (t, 2H), 2.99 (t, 2H), 2.25 (br, 1H), 0.84 (s, 9H), 0.00 (s, 6H) ppm. LRMS: m/z 299 [M + H]⁺.

2-[(2-[(*tert*-Butyl(dimethyl)silyl]oxy)ethyl]thio]benzaldehyde (21b**).** To a solution of **23** (5.90 g, 19.87 mmol) in dichloromethane (100 mL) was added barium permanganate (25.32 g, 99.27 mmol), and the mixture was stirred at room temperature for 24 h. The mixture was filtered through Celite and concentrated in vacuo. Crude analysis indicated that significant starting material remained. The residue was then diluted with dichloromethane (100 mL), and manganese dioxide (25 g, 288 mmol) was added. The mixture was heated to reflux overnight. The mixture was allowed to cool to room temperature and then filtered through Celite. The residue was concentrated in vacuo to give a purple oil (3.66 g, 62%). ¹H NMR (400 MHz, CDCl₃) δ 10.39 (s, 1H), 7.78 (d, 1H), 7.46 (d, 1H), 7.24–7.28 (m, 1H), 3.78 (t, 2H), 3.05 (t, 2H), 0.84 (s, 9H), 0.00 (s, 6H). LRMS: m/z 297 [M + H]⁺.

2-[(2-[(*tert*-Butyl(dimethyl)silyl]oxy)ethyl]thio]benzaldehyde (5-bromopyridin-2-yl)hydrazone (15a**).** To a solution of **21b** (3.61 g, 12.24 mmol) in ethanol (10 mL) was added (5-bromopyridin-2-yl)hydrazine (2.30 g, 12.24 mmol), and the mixture was heated to reflux for 3 h. The solvent was then removed in vacuo to give the product as a pink solid (5.63 g, 99%). ¹H NMR (400 MHz, CDCl₃) δ 9.20 (br, 1H), 8.39 (s, 1H), 8.13 (d, 1H), 7.88–7.91 (m, 1H), 7.66 (dd, 1H), 7.43–7.45 (m, 1H), 7.31 (d, 1H), 7.21–7.28 (m, 1H), 3.73 (t, 2H), 2.98 (t, 2H), 2.74–2.96 (br, 1H), 0.84 (s, 9H), 0.00 (s, 6H) ppm. LRMS: m/z 466–468 [M + H]⁺.

6-Bromo-3-{2-[(2-[(*tert*-butyl(dimethyl)silyl]oxy)ethyl]thio]phenyl}[1,2,4]triazolo[4,3-*a*]pyridine (16a**).** To a solution of **15a** (5.63 g, 12.08 mmol) in dichloromethane (50 mL) and methanol (15 mL) was added iodobenzene diacetate (4.67 g, 14.50 mmol), and the mixture was stirred at room temperature overnight. The mixture was then diluted with dichloromethane (50 mL), and the mixture was washed with sodium hydroxide solution (1M, 100 mL), brine (100 mL), and subsequently dried (MgSO₄). The organics were then concentrated in vacuo and purified by column chromatography on silica gel, eluting with a gradient of ethyl acetate in heptane from 0% to 100%. Fractions containing product were concentrated in vacuo to leave a pink oil (4.30 g, 77%). ¹H NMR (400 MHz, CDCl₃) δ 7.92 (dd, 1H), 7.76 (dd, 1H), 7.65 (dd, 1H), 7.57–7.58 (m, 2H), 7.36–7.43 (m, 2H), 3.69 (t, 2H), 2.93 (t, 2H), 0.84 (s, 9H), 0.00 (s, 6H) ppm. LRMS: m/z 464–466 [M + H]⁺.

2-[(3-{2-[(2-[(*tert*-Butyl(dimethyl)silyl]oxy)ethyl]thio]phenyl}[1,2,4]triazolo[4,3-*a*]pyridin-6-yl]thio]phenyl]methanol (17a**).** A solution of **16a** (2.0 g, 4.31 mmol) in *N,N*-dimethylformamide (70 mL) was degassed with argon. 2-Mercaptobenzyl alcohol (724 mg, 5.17 mmol), cesium carbonate (2.81 g, 8.62 mmol), and [1,1'-bis-(diphenylphosphino)ferrocene]dichloropalladium(II) (169 mg, 431 μ mol) were then added, and the mixture was degassed an additional time. The mixture was then heated to 90 °C for 4 h. The mixture was concentrated in vacuo, and the residue was partitioned between ethyl acetate (50 mL) and water (100 mL). The aqueous phase was then re-extracted with ethyl acetate (50 mL). The combined organics were washed with brine (100 mL), dried (MgSO₄), and concentrated in vacuo. The residue was purified by column chromatography on silica gel, eluting with ethyl acetate in heptane in a gradient from 0% to 100%. Fractions containing product were concentrated in vacuo to leave a brown gum (1.32 g, 59%). ¹H NMR (400 MHz, CDCl₃) δ 7.78 (d, 1H), 7.24 (d, 1H), 7.52–7.64 (m, 4H), 7.38 (dd, 1H), 7.33 (dd, 1H), 7.27–7.30 (m, 2H), 7.17 (dd, 1H), 4.85 (s, 2H), 3.67 (t, 2H), 2.90 (t, 2H), 0.84 (s, 9H), 0.00 (s, 6H) ppm. LRMS: m/z 524 [M + H]⁺.

1-{2-[(3-{2-[(2-{[*tert*-Butyl(dimethyl)silyl]oxy}ethyl)thio]phenyl}[1,2,4]triazolo[4,3-*a*]pyridin-6-yl)thio]phenyl}metanamine (**2a**). To a solution of **17a** (1.32 g, 2.52 mmol) in dichloromethane (20 mL) was added *N,N*-diisopropylethylamine (0.88 mL, 5.05 mmol) followed by methanesulfonic anhydride (666 mg, 3.79 mmol), and the mixture was stirred for 2 h at room temperature. The solution was then poured into a solution of methanolic ammonia (7 M, 36 mL, 252.2 mmol), and the mixture was stirred for 4 h. The solvent was removed in vacuo, and the residue was partitioned between ethyl acetate (50 mL) and ammonium hydroxide (20 mL). The organics were then washed with brine (50 mL), dried (MgSO₄), and concentrated in vacuo. Purification was effected using column chromatography on silica gel, eluting from 0% to 10% methanol in (99:1) ethyl acetate with ammonia. Fractions containing product were concentrated in vacuo to leave a brown oil (904 mg, 68%). ¹H NMR (400 MHz, CDCl₃) δ 7.82–7.83 (m, 1H), 7.76 (dd, 1H), 7.63 (dd, 1H), 7.58 (dd, 1H), 7.52 (dd, 1H), 7.45 (d, 1H), 7.39 (dd, 1H), 7.27–7.32 (m, 1H), 7.21–7.23 (m, 2H), 7.16 (dd, 1H), 4.07 (s, 2H), 3.66 (t, 2H), 2.90 (t, 2H), 0.85 (s, 9H), 0.00 (s, 6H) ppm. LRMS: *m/z* 523 [M + H]⁺.

2-Chloro-4-hydrazinophenol (4b). To a suspension of 4-amino-2-chlorophenol (25 g, 174 mmol) in water (40 mL) was added concentrated hydrochloric acid (63 mL, 783 mmol). The mixture was cooled to –10 °C under nitrogen. A solution of sodium nitrite (12.0 g, 174 mmol) in water (35 mL) was added dropwise. After addition was complete the mixture was stirred for an additional 30 min at –10 °C. Tin(II) chloride dehydrate (98.1 g, 435 mmol) was dissolved in 6 M hydrochloric acid (100 mL), and the diazotization mixture was poured into this solution. The mixture was stirred for 3.5 h at –10 °C. The solids were then filtered off and dried overnight. The material was not purified further but carried over into the next step. LRMS: *m/z* 159 [M + H]⁺.

4-(5-Amino-3-*tert*-butyl-1H-pyrazol-1-yl)-2-chlorophenol (12). To a solution of **4b** (174 mmol) (carried over from the previous step) in ethanol (250 mL) was added 4,4-dimethyl-3-oxopentanitrile (21.9 g, 174 mmol), and the mixture was heated to reflux overnight. The solvent was removed in vacuo. The residue was then triturated using diethyl ether (125 mL) and heptane (250 mL). After the mixture was stirred vigorously for 2 h a fine powder was obtained. The powder was filtered off and resuspended in diethyl ether (100 mL) and heptane (200 mL), and the mixture was stirred for an additional 2 h. The solid was filtered off and dried in a vacuum oven (40 °C) to afford the desired compound as a brown solid (22 g, 48% over two steps). ¹H NMR (400 MHz, DMSO-*d*₆) δ 11.10 (br, 1H), 7.10–7.67 (m, 3H), 5.61 (s, 1H), 1.28 (s, 9H) ppm. LRMS: *m/z* 266–268 [M + H]⁺.

3-*tert*-Butyl-1-(4-{[*tert*-butyl(dimethyl)silyl]oxy}-3-chlorophenyl)-1H-pyrazol-5-amine (3f). To a solution of **12** (40 g, 0.15 mol) in *N,N*-dimethylformamide (100 mL) were added *tert*-butyl-(dimethyl)silyl chloride (23.8 g, 0.16 mol) and imidazole (11.2 g, 0.17 mol). The mixture was then stirred at room temperature overnight. The reaction was quenched by addition of methanol (40 mL), and subsequently the mixture was concentrated in vacuo. The residue was partitioned between ethyl acetate (300 mL) and aqueous saturated sodium bicarbonate solution (100 mL). The aqueous was then re-extracted with ethyl acetate (2 × 300 mL). The organic washes were then combined and dried (Na₂SO₄). After concentration in vacuo, the residue was purified by column chromatography on silica gel, eluting with ethyl acetate in hexane (1:6). Fractions containing product were concentrated in vacuo and then crystallized from ethyl acetate and hexane, giving fine white needle crystals (9.6 g, 17%). ¹H NMR (400 MHz, DMSO-*d*₆) δ 7.64 (d, 1H), 7.48 (dd, 2H), 7.10 (d, 1H), 5.41 (s, 1H), 5.22 (br, 2H), 1.24 (s, 9H), 1.05 (s, 9H), 0.29 (s, 6H) ppm. LRMS: *m/z* 380–382 [M + H]⁺.

Phenyl [3-*tert*-Butyl-1-(4-{[*tert*-butyl(dimethyl)silyl]oxy}-3-chlorophenyl)-1H-pyrazol-5-yl]carbamate (31c). To a 0 °C cooled solution of **3f** (4.0 g, 10.5 mmol) in tetrahydrofuran (30 mL) was added pyridine (1.20 mL, 14.7 mmol) followed by dropwise addition of

phenyl chloroformate (1.46 mL, 11.6 mmol). After addition was complete the mixture was allowed to warm to room temperature for 3 h. The mixture was then partitioned between ethyl acetate (100 mL) and water (100 mL). The organics were separated, washed with brine (40 mL), dried (Na₂SO₄), and concentrated in vacuo to yield an orange oil. The oil was triturated with heptane (60 mL) and the triturate stirred for 1 h. The desired product was then filtered off as a white solid (4.5 g, 86%). ¹H NMR (400 MHz, CDCl₃) δ 7.55 (d, 1H), 7.37–7.42 (m, 2H), 7.27–7.32 (m, 2H), 7.23–7.26 (m, 1H), 7.10–7.18 (m, 2H), 7.02 (d, 1H), 6.46 (br, 1H), 1.36 (s, 9H), 1.07 (s, 9H), 0.28 (s, 6H) ppm. LRMS: *m/z* 500 [M + H]⁺.

1-[3-*tert*-Butyl-1-(3-chloro-4-hydroxyphenyl)-1H-pyrazol-5-yl]-3-{2-[(3-{2-[(2-{[*tert*-butyl(dimethyl)silyl]oxy}ethyl)thio]phenyl}[1,2,4]triazolo[4,3-*a*]pyridin-6-yl)thio]benzyl}urea (36). To a solution of **31c** (100 mg, 0.2 mmol) in dimethylsulfoxide (2 mL) was added **2a** (105 mg, 0.2 mmol), and the mixture was stirred overnight at room temperature. The mixture was diluted with ethyl acetate (30 mL) and water (30 mL). The organics were separated, washed with brine (20 mL), dried over (Na₂SO₄), filtered, and concentrated in vacuo. The residue was purified using column chromatography on silica gel, eluting with ethyl acetate in cyclohexane, 0–100%. Product containing fractions were combined and concentrated in vacuo to give the desired product as a white solid (110 mg, 68%). ¹H NMR (400 MHz, methanol-*d*₄) δ 7.78–7.82 (m, 1H), 7.72–7.76 (m, 2H), 7.62–7.67 (m, 1H), 7.58 (dd, 1H), 7.29–7.49 (m, 7H), 7.21–7.24 (m, 1H), 7.02 (d, 1H), 6.28 (s, 1H), 4.51 (s, 1H), 3.73 (t, 2H), 3.00 (t, 2H), 1.34 (s, 9H), 0.84 (s, 9H), 0.00 (s, 6H) ppm. LRMS: *m/z* 814 [M + H]⁺.

1-[3-*tert*-Butyl-1-(3-chloro-4-hydroxyphenyl)-1H-pyrazol-5-yl]-3-{2-[(3-{2-[(2-hydroxyethyl)thio]phenyl}[1,2,4]triazolo[4,3-*a*]pyridin-6-yl)thio]benzyl}urea (1ab). To a solution of **36** (90 mg, 0.1 mmol) in methanol (10 mL) was added triethylamine trihydrofluoride (18 μL, 0.1 mmol), and the mixture was stirred at room temperature overnight. The mixture was concentrated in vacuo. Then 7 M methanolic ammonia (20 mL) was added, and the reaction mixture was concentrated again in vacuo. The residue was preabsorbed onto silica gel and purified using column chromatography, eluting with a gradient of ammonia in dichloromethane (0.3:99.7) to a mixture of dichloromethane, methanol, and ammonia (94.5:5:0.5). Product containing fractions were combined and concentrated in vacuo to give the desired product as a white solid (51 mg, 73%). ¹H NMR (400 MHz, methanol-*d*₄) δ 7.72–7.76 (m, 1H), 7.64–7.68 (m, 2H), 7.58–7.63 (m, 1H), 7.53 (d, 1H), 7.37–7.44 (m, 3H), 7.23–7.36 (m, 4H), 7.17 (d, 1H), 6.97 (d, 1H), 6.23 (s, 1H), 4.46 (s, 2H), 3.56 (d, 2H), 2.94 (d, 2H), 1.29 (s, 9H) ppm. LRMS: *m/z* 700 [M + H]⁺. Anal. (C₃₅H₃₄ClN₇O₃S₂) C, H, N.

■ ASSOCIATED CONTENT

Supporting Information. Additional experimental procedures and analytical data for intermediates and final compounds. This material is available free of charge via the Internet at <http://pubs.acs.org>.

Accession Codes

¹PDB codes are the following: 2yis for **1ab**, 2yiw for **1a**, and 2yix for **41**.

■ AUTHOR INFORMATION

Corresponding Author

*To whom correspondence should be addressed. Phone: +44 1304 643497. Fax: +44 1304 651987. E-mail: david.millan@gmail.com.

ACKNOWLEDGMENT

We thank Jonathan Duckworth for assistance with ADME experiments. Deborah Bruce, Iva Navratilova, and Klaus Rumpel are thanked for assistance with Biacore generated data. Suengil Han, Eric Marr, Marie Anderson, and Stephen Irving are thanked for assistance with X-ray crystallographic data. William Hood is thanked for help with progression curve experiments and analysis. Joe Monahan is also thanked for useful advice and guidance.

DEDICATION

[†]This paper is dedicated to the memory of Mark H. Stefaniak.

ABBREVIATIONS USED

ATP, adenosine triphosphate; CNS, central nervous system; CRP, C-reactive protein; COPD, chronic obstructive pulmonary disease; CYP, cytochrome P450; DDI, drug–drug interaction; DoA, duration of action; FEV₁, forced expiratory volume in 1 s; hERG, human ether-a-go-go-related gene; HLM, human liver microsomes; IL-1 β , interleukin 1 β ; IL-6, interleukin 6; LPS, lipopolysaccharide; MMP-9, matrix metalloprotease 9; MINK, misshapen NIK related kinase 1; MAP, mitogen activated kinase; PBMC, peripheral blood mononuclear cells; PDB, Protein Data Bank; P-gp, P-glycoprotein; PDE4, phosphodiesterase 4; PPB, plasma protein binding; RA, rheumatoid arthritis; Ro5, rule-of-five; SLF, simulated lung fluid; SAR, structure–activity relationship; TBDMS, *tert*-butyldimethylsilyl; THP, tetrahydropyran-2-yl; TNF- α , tumor necrosis factor α ; VEGFR1, vascular endothelial growth factor receptor 1

REFERENCES

- (1) Dinarello, C. A. Inflammatory cytokines: interleukin-1 and tumour necrosis factor as effector molecules in autoimmune diseases. *Curr. Opin. Immunol.* **1991**, *3*, 941–948.
- (2) Lee, S. J.; Kavanaugh, A. A. Pharmacological treatment of established rheumatoid arthritis. *Best Pract. Res., Clin. Rheumatol.* **2003**, *17*, 811–829.
- (3) Weisman, M.; Furst, D.; Schiff, M.; et al. A Double-Blind, Placebo Controlled Trial of VX-745, an Oral p38 Mitogen-Activated Protein Kinase (MAPK) Inhibitor in Patients with Rheumatoid Arthritis (RA). Presented at the Annual Congress of the European League against Rheumatism, Stockholm, Sweden, Jun 12–15, 2002; FRI0018.
- (4) Schreiber, S.; Feagan, B.; D'Haens, G.; Colombel, J.-F.; Geboes, K.; Yurcov, M.; Isakov, V.; Golovenko, O.; Bernstein, C. N.; Ludwig, D.; Winter, T.; Meier, U.; Yong, C.; Steffgen, J. Oral p38 mitogen-activated protein kinase inhibition with BIRB 796 for active Crohn's disease: a randomized, double-blind, placebo-controlled trial. *Clin. Gastroenterol. Hepatol.* **2006**, *4*, 325–334.
- (5) Goldstein, D. M.; Kuglstatler, A.; Lou, Y.; Soth, M. J. Selective p38 α inhibitors clinically evaluated for the treatment of chronic inflammatory disorders. *J. Med. Chem.* **2010**, *53*, 2345–2353.
- (6) Vertex Pharmaceuticals Inc: Vertex moves to re-allocate resources from VX-745 in p38 MAP kinase program to accelerate development of second generation drug candidates VX-702 and VX-850. Press Release, September 24, 2001.
- (7) Wood; Yong; Madwed; Gupta, A. Safety, pharmacokinetics and pharmacodynamics of an oral p38 MAP kinase inhibitor (BIRB 796 BS), administered once daily for 7 days. *J. Allergy Clin. Immunol.* **2002**, *109*, 993.
- (8) Boehringer Ingelheim. <http://www.boehringer-ingenheim.com> (accessed April 13, 2011).
- (9) Mannino, D. M.; Buist, A. S. Global burden of COPD: risk factors, prevalence, and future trends. *Lancet* **2007**, *370*, 765–773.
- (10) Barnes, P. J.; Adcock, I. M. Glucocorticoid resistance in inflammatory diseases. *Lancet* **2009**, *373*, 1905–1917.

- (11) Renda, T.; Baraldo, S.; Pelaia, G.; Bazzan, E.; Turato, G.; Papi, A.; Maestrelli, P.; Maselli, R.; Vatrella, A.; Fabbri, L. M.; Zuini, R.; Marsico, S. A.; Saetta, M. Increased activation of p38 MAPK in COPD. *Eur. Respir. J.* **2008**, *31*, 62–69.

- (12) Underwood, D. C.; Osborn, R. R.; Kotzer, C. J.; Adams, J. L.; Lee, J. C.; Webb, E. F.; Carpenter, D. C.; Bochnowicz, S.; Thomas, H. C.; Hay, D. W. P.; Griswold, D. E. SB 217063, a potent p38 MAP kinase inhibitor, reduces inflammatory cytokine production, airways eosinophil infiltration, and persistence. *J. Pharmacol. Exp. Ther.* **2000**, *293*, 281–288.

- (13) Medicherla, S.; Fitzgerald, M.; Spicer, D.; Woodman, P.; Ma, J. Y.; Kapoun, A. M.; Chakravarty, S.; Dugar, S.; Protter, A. A.; Higgins, L. S. p38 α selective MAP kinase inhibitor, SD-282, reduces inflammation in a sub-chronic model of tobacco smoke-induced airway inflammation. *J. Pharmacol. Exp. Ther.* **2008**, *324*, 921–929.

- (14) Duan, W.; Chan, J. H.; McKay, K.; Crosby, J. R.; Choo, H. H.; Leung, B. P.; Karras, J. G.; Wong, W. S. F. Inhaled p38 α mitogen-activated protein kinase antisense oligonucleotide attenuates asthma in mice. *Am. J. Respir. Crit. Care Med.* **2005**, *171*, 571–578.

- (15) Array Biopharm. <http://www.arraybiopharma.com> (accessed April 13, 2011).

- (16) ClinicalTrials.gov. <http://www.clinicaltrials.gov> (accessed April 13, 2011).

- (17) (a) MacNee, W.; Allan, R.; Jones, I.; De Salvo, M. C.; Tan, L. A Randomised, Placebo Controlled Trial of 6 Weeks' Treatment with a Novel Oral p38 Inhibitor in Patients with COPD. Presented at the European Respiratory Society Meeting, Barcelona, Spain, 2010. (b) Selness, S. R.; Devraj, R. V.; Devadas, B.; Walker, J. K.; Boehm, T. L.; Durley, R. C.; Shieh, H.; Xing, L.; Rucker, P. V.; Jerome, K. D.; Benson, A. G.; Marrufo, L. D.; Madsen, H. M.; Hitchcock, J.; Owen, T. J.; Christie, L.; Promo, M. A.; Hickory, B. S.; Alvira, E.; Naing, W.; Blevis-Bal, R.; Messing, D.; Yang, J.; Mao, M. K.; Yalamanchili, G.; Vonder Embse, R.; Hirsch, J.; Saabye, M.; Bonar, S.; Webb, E.; Anderson, G.; Monahan, J. B. Discovery of PH-797804, a highly selective and potent inhibitor of p38 MAP kinase. *Bioorg. Med. Chem. Lett.* **2011**, *21*, 4066–4071.

- (18) Chopra, P.; Kanoje, V.; Semwal, A.; Ray, A. Therapeutic potential of inhaled p38 mitogen-activated protein kinase inhibitors for inflammatory pulmonary diseases. *Expert Opin. Invest. Drugs* **2008**, *17*, 1411–1425.

- (19) Millan, D. S. What is the potential for inhaled p38 inhibitors in the treatment of chronic obstructive pulmonary disease? *Future Med. Chem.* **2011**, *3*, 1635–1645.

- (20) Glossop, P. A.; Lane, C. A. L.; Price, D. A.; Bunnage, M. E.; Lewthwaite, R. A.; James, K.; Brown, A. D.; Yeadon, M.; Perros-Huguet, C.; Trevelthick, M. A.; Clarke, N. P.; Webster, R.; Jones, R. M.; Burrows, J. L.; Feeder, N.; Taylor, S. C. J.; Spence, F. J. Inhalation by design: novel ultra-long-acting β 2-adrenoreceptor agonists for inhaled once-daily treatment of asthma and chronic obstructive pulmonary disease that utilize a sulfonamide agonist headgroup. *J. Med. Chem.* **2010**, *53*, 6640–6652.

- (21) Lipinski, C. A.; Lombardo, F.; Dominy, B. W.; Feeney, P. J. Experimental and computational approaches to estimate solubility and permeability in drug discovery and development settings. *Adv. Drug Delivery Rev.* **1997**, *23*, 3–25.

- (22) Regan, J.; Capolino, A.; Cirillo, P. F.; Gilmore, T.; Graham, A. G.; Hickey, E.; Kroe, R. R.; Madwed, M.; Moriak, M.; Nelson, R.; Pargellis, C. A.; Swinamer, A.; Torcellini, C.; Tsang, M.; Moss, N. Structure–activity relationships of the p38 α MAP kinase inhibitor 1-(5-*tert*-butyl-2-*p*-tolyl-2H-pyrazol-3-yl)-3-[4-(2-morpholin-4-yl-ethoxy)-naphthalen-1-yl]urea (BIRB 796). *J. Med. Chem.* **2003**, *46*, 4676–4686.

- (23) Regan, J.; Pargellis, C. A.; Cirillo, P. F.; Gilmore, T.; Hickey, E. R.; Peet, G. W.; Proto, A.; Swinamer, A.; Moss, N. The kinetics of binding to p38 MAP kinase by analogues of BIRB 796. *Bioorg. Med. Chem. Lett.* **2003**, *13*, 3101–3104.

- (24) McClure, K. F.; Abramov, Y. A.; Laird, E. R.; Barberia, J. T.; Cai, W.; Carty, T. J.; Cortina, S. R.; Danley, D. E.; Dipesa, A. J.; Donahue, K. M.; Dombroski, M. A.; Elliott, N. C.; Gabel, C. A.; Han, S.; Hynes, T. R.; LeMotte, P. K.; Mansour, M. N.; Marr, E. S.; Letavic, M. A.; Pandit, J.; Ripin, D. B.; Sweeney, F. J.; Tan, D.; Tao, Y. Theoretical and

experimental design of atypical kinase inhibitors: application to p38 MAP kinase. *J. Med. Chem.* **2005**, *48*, 5728–5737.

(25) Braganza, J. F.; Letavic, M. A.; McClure, K. F. Preparation of Triazolo[4,3-*a*]pyridines as MAP Kinases, in Particular p38 Kinase Inhibitors, and Their Use as Antiinflammatory Agents. WO2004072072, 2004.

(26) Liu, H.; Kuhn, C.; Feru, F.; Jacques, S. L.; Deshmukh, G. D.; Ye, P.; Rennie, G. R.; Johnson, T.; Kazmirski, S.; Low, S.; Coli, R.; Ding, Y.-H.; Cheng, A. C.; Tecele, H.; English, J. M.; Stanton, R.; Wu, J. C. Enhanced selectivity profile of pyrazole-urea based DFG-out p38 α inhibitors. *Bioorg. Med. Chem. Lett.* **2010**, *20*, 4885–4891.

(27) Fisher, M. B.; Paine, M. F.; Strelevitz, T. J.; Wrighton, S. A. The role of hepatic and extrahepatic UDP-glucuronosyltransferases in human drug metabolism. *Drug Metab. Rev.* **2001**, *33*, 273–297.